2024

INVESTIGATING A MAJOR 16S rRNA FOLDING EVENT IN THE ASSEMBLY OF THE 30S RIBOSOMAL SUBUNIT

Brenna Levesque
University of Rhode Island, brennalevesque26@gmail.com

INVESTIGATING A MAJOR 16S rRNA FOLDING EVENT IN THE ASSEMBLY OF THE 30S RIBOSOMAL SUBUNIT

BY

BRENNA LEVESQUE

A THESIS SUBMITTED IN PARTIAL FULFILLMENT OF THE REQUIREMENTS FOR THE DEGREE OF

MASTER OF SCIENCE

IN

BIOLOGICAL AND ENVIRONMENTAL SCIENCES

UNIVERSITY OF RHODE ISLAND

2024

MASTER OF SCIENCE THESIS

OF

BRENNA LEVESQUE

APPROVED:

Thesis Committee:

Major Professor Steven Gregory

Kathryn Ramsey

Alison Roberts

Brenton DeBoef
DEAN OF THE GRADUATE SCHOOL

UNIVERSITY OF RHODE ISLAND
2024

Abstract

The ribosome is the large macromolecular machine responsible for protein synthesis, the final step of gene expression, in all cells. It is made up of ribosomal proteins (r-proteins) and ribosomal RNA (rRNA), and how these many components assemble into a functionally active particle is only poorly understood. In this thesis, I have used the extremely thermophilic bacterium *Thermus thermophilus* as a model system to study the role of a specific ribosomal protein, bS20, in 30S ribosomal subunit assembly. Results from these experiments suggest a potential role in ribosome function once assembly has occurred.

All ribosomes are composed of two subunits, and in bacteria these are the 30S and 50S subunits, which combine to make up the full 70S ribosome. The larger 50S subunit consists of 23 rRNA, 5S rRNA, and typically 33 r-proteins (the actual number varies among species); this larger subunit is responsible for catalyzing peptide bond formation, the reaction linking amino acids together. The smaller 30S subunit consists of 16S rRNA and typically 21 r-proteins and is responsible for reading the genetic code as expressed by messenger RNA (mRNA). The interface between the two subunits contains three tRNAs that act as a bridge between the mRNA and growing amino acid chain.

While a great deal is known about the final structure of the ribosome and its function during protein synthesis, much less is known about how the ribosome assembles and the impact of assembly defects on protein synthesis. The broader goal of this project is to identify interactions that are critical for major

16S rRNA folding events that must occur during 30S ribosomal subunit assembly. To help bring some of these interactions to light, I have focused on ribosomal proteins and how they contribute to this process. I have chosen to compare two ribosomal proteins, uS17 and bS20, and the effects resulting from deletion of either of the genes encoding them. These proteins are located near one another in the 30S ribosomal subunit but are involved in distinct RNA-RNA interactions. In constructing and characterizing a mutant lacking bS20, I found that this protein is not essential for viability. However, the severe growth phenotype of the mutant suggests important structural or functional roles for this protein. An increase in sensitivity to the antibiotic streptomycin also suggests a defect in decoding accuracy, consistent with observations with other species. These results form the foundation for a more detailed analysis of the role of bS20 in ribosome assembly and protein synthesis.

Acknowledgements

I would like to express my sincere gratitude to my major professor Dr. Steven Gregory. His support and abundance of knowledge were greatly appreciated throughout my time in his lab and my graduate school career. I also thank him for helping to instill a love of old movies and a strong work ethic that revolves around planning, prepping, and multitasking. I am honored to be his second master's student to graduate at the University of Rhode Island and I wish all the best to him, his lab, and all the future graduate and undergraduate students that are able to work with him.

I would like to thank the members of my committee Dr. Kathryn Ramsey and Dr. Alison Roberts for their willingness to participate in my journey to getting my master's degree. Their interest in my project, suggestions, and the time/effort they put in for me have been incredibly appreciated. Thank you to Dr. Ramsey for all her help during lab meetings and when I took her class. Thank you to Dr. Roberts for being willing to be a part of my committee on a very short notice, for her quick communication and helpful outside perspective suggestions.

Thank you to the current and former lab members who were all a pleasure to work with, including: Kamila Guerra, Julia Highcove, Chris Rodman, Julia Hobaugh, Abigail Wilson, and especially Erin Killeavy who has been the most incredible mentor and friend throughout my graduate school career. I would like to thank Janet Atoyan for all her help with sequencing and running sucrose gradients at the URI Genomics and Sequencing Center (INBRE).

Lastly, I would like to thank you the faculty and graduate students in the Cell and Molecular Biology department, as well as my coworkers in the Anatomy and Physiology course. Thank you all for providing a welcoming and supporting community throughout my time at URI. I could not have asked for a better group of cohorts and fellow scientists.

Table of contents

ABSTRACT ii

ACKNOWLEDGEMENTS iv

TABLE OF CONTENTS vi

LIST OF TABLES ix

LIST OF FIGURES xi

CHAPTER 1 1

INTRODUCTION 1

CHAPTER 2 4

REVIEW OF LITERATURE 4

CHAPTER 3 6

METHODOLOGY 6

CHAPTER 4 8

FINDINGS 8

CHAPTER 5 10

CONCLUSION 10

APPENDICES 12

List of tables

TABLE PAGE

Table 1. Oligonucleotides used in this study. 29

Table 2. Plasmids used in this study 30

Table 3. Bacterial strains used in this study 30

Table 4. Antibiotics and their targets 42

Table 5. bS20-16S interactions in *T. thermophilus* 51

List of figures

FIGURE PAGE

Figure 1. Domain organization of the 30S ribosomal subunit. 2

Figure 2. The 30S ribosomal subunit assembly map 5

Figure 3. 30S subunit surface rendering 8

Figure 4. Surface rendering of *T. thermophilus* 30S subunit 11

Figure 5. Binding sites for uS17 and bS20 on 16S rRNA 12

Figure 6. Schematic used to replace the bS20 encoding gene *rpsT* 32

Figure 7. Plasmid construct of the *rpsT* deletion mutant (Δ*rpsT::htk)* 33

Figure 8. Diagnostic PCR to confirm deletion of *rpsT.* 36

Figure 9. Plasmid construct of the bS20 expression plasmid 38

Figure 10. Growth phenotype of the Δ*rpsT::htk* deletion mutation 40

Figure 11. Bar graph showing average zones of inhibition of wild type and bS20 knockout strain in antibiotic presence 44

Figure 12. ΔbS20(pSAD1-bS20), wild type, and ΔbS20 growth at various temperatures 47

Figure 13. ΔbS20(pSAD1-bS20, wild type complementation growth at 55 & 65°C……..... 48

Figure 14. Potential long-range effects of bS20 deficiency……..57

Figure 15. Antibiotics binding to 16S rRNA h44 58

CHAPTER 1

Introduction & review of literature

The ribosome is the ribonucleoprotein complex responsible for protein synthesis, the final stage of gene expression in all cells. It is made up of ribosomal proteins (r-proteins) and ribosomal RNA (rRNA). The fully assembled 70S ribosome is composed of two subunits. In bacteria, the 50S subunit consists of around 120 nucleotides of 5S rRNA, 2900 nucleotides of 23S rRNA, and typically 33 proteins. This subunit is charged with catalyzing peptide bond formation, which is what links the growing amino acid chain together. The smaller 30S subunit consists of around 1540 nucleotides of 16S rRNA and typically 21 proteins. It is tasked with reading the genetic code as expressed by the messenger RNA (mRNA). It also binds the mRNA, the initiation factors, and the 50S subunit; it is directly responsible for selection of correct tRNA (Schmeing & Ramakrishnan, 2009). The fully assembled 70S ribosome has a molecular weight of approximately 2.5 MDa, two-thirds of which due to the rRNA and the remaining one-third due to the proteins, and a diameter of about twenty-five nanometers (Noeske & Cate, 2012).

The 30S subunit is organized into three domains (body, platform, head), each corresponding to a morphological feature identified in electron microscopy studies in the 1970s (Lake, 1976). These domains correspond to the 5', central, and 3' domains of 16S rRNA, respectively (Figure 1).

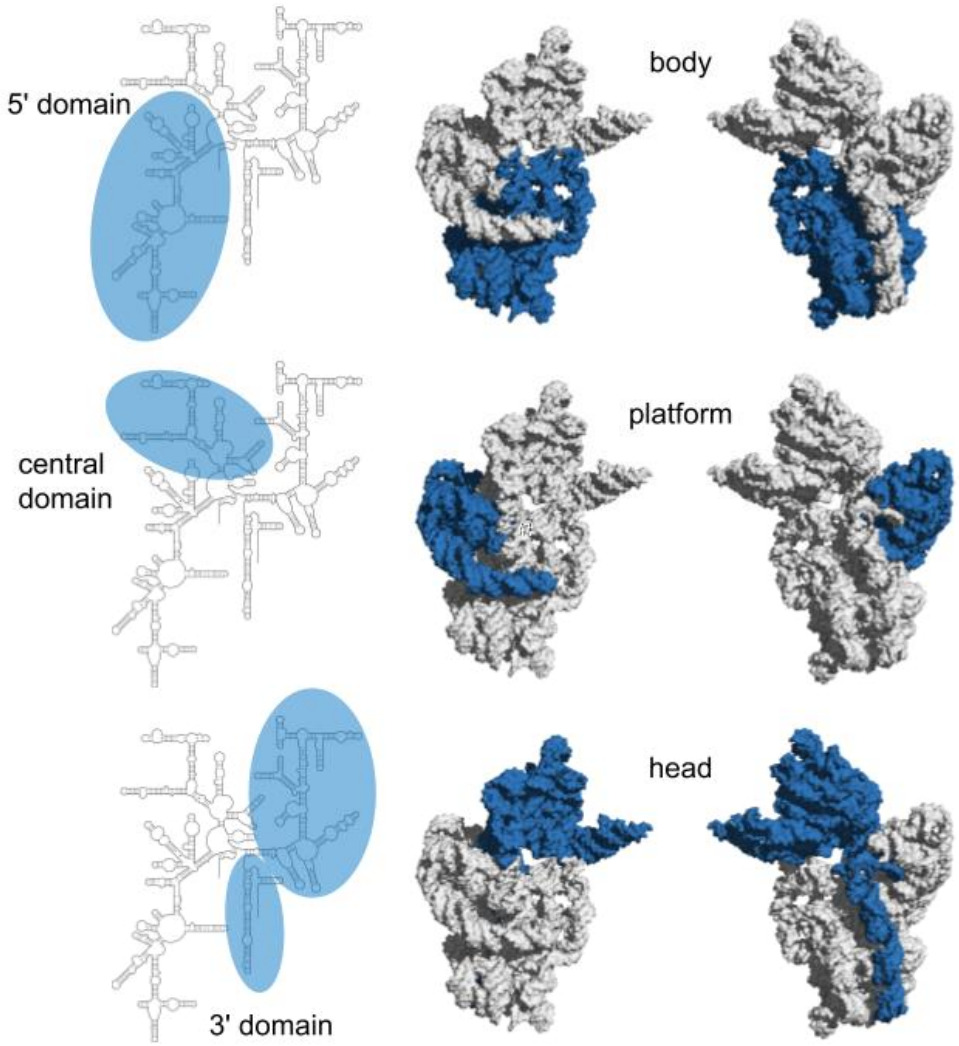

Figure 1. Domain organization of the 30S ribosomal subunit. (Left) Secondary structure map of *T. thermophilus* 16S rRNA, with individual domains highlighted. (Center and Right) Surface renderings of *T. thermophilus* 16S rRNA with individual domains colored skyblue and designated according to early electron microscopy observations of 30S subunits (Lake 1976). Surfaces are viewed from the solvent side (middle column) or subunit interface side (right column). Surface renderings generated with PyMOL using pdb entry 4y4p (Polikanov et al., 2015).

Early research on ribosomes revolved around identification and characterization of the ribosomal proteins that make up the ribosome (Waller, 1964; Watson, 1964; Mizushima & Nomura, 1970; Nomura, 1970; Wittmann, 1975; Warner & Gorenstein, 1978). This was followed by the determination of the complete sequences of the 16S rRNA from the mesophilic bacterium *Escherichia coli* (Brosius *et al.,* 1978) and the extremely thermophilic bacterium *Thermus thermophilus* (Murzina *et al.,* 1988). 16S rRNA secondary structures were determined by comparative sequence analysis (Noller & Woese, 1981; Cannone *et al.*, 2002).

Since then, advances in X-ray crystallography and cryo-electron microscopy (cryo-EM) have led to the determination of high-resolution structures of the ribosome at various stages of protein synthesis (Frank, 2003; Noller, 2005; Ramakrishnan, 2009; Steitz, 2009; Yonath, 2009), some at atomic resolution (Watson *et al*., 2020; Fromm *et al*., 2023). These high-resolution images have led to a detailed understanding of how the ribosome performs protein synthesis. While much is known about the structure and function of the ribosome, much remains to be learned about how it assembles from its constituent proteins and rRNAs. This thesis will focus on helping bring some light to the assembly process of the 30S subunit.

Assembly of the 30S subunit

While a great deal is known about the functions of the ribosome during protein synthesis, ribosome assembly remains a major unresolved question in molecular biology. Ribosome synthesis involves a large investment of cellular resources and must be tightly regulated, for any mistakes can poison protein synthesis (Woodson, 2008).

Early work on *E. coli* ribosome assembly (reviewed by Nomura and Held, 1974) used *in vitro* reconstitution to show that ribosomal proteins are incorporated into the assembling 30S subunit based in a hierarchy (Figure 2). The primary binding proteins (uS17, bS20, uS4, uS8, uS15, uS7) are the first to assemble and bind directly to the 16S rRNA, while the secondary proteins (bS16, bS6, bS18, uS9, uS13, uS19) depend on prior binding of one or more primary binding proteins, and lastly the tertiary proteins (uS12, uS5, uS11, bS21, uS10, uS14, uS3, uS2) need a temperature-dependent conformational step to assemble (Held e*t al.,* 1974).

This hierarchy leads to cooperativity in assembly. As the rRNA starts to become more ordered, proteins begin to assemble and in conjunction with an rRNA folding pathway (Held *et al*., 1973; Culver, 2003; Williamson, 2003). The proteins drive forward the formation of the ribosome's native conformation to prevent the formation of misfolded rRNA intermediates (Adilakshmi *et al.,* 2008). While most ribosomal proteins in *E. coli* are essential, bS6, uS9, uS13, uS15, uS17, and bS20 are dispensable. Knockout mutants lacking any of these proteins are still viable and able to form slow-growing, small colonies; some mutants also show temperature-sensitive or cold-sensitive phenotypes. (Guthrie, Nashimoto, & Nomura, 1969;

Dabbs 1991; Ramakrishnan, 2002). The dispensable proteins are not situated near any important functional centers of the ribosome, and therefore may be why they are not essential.

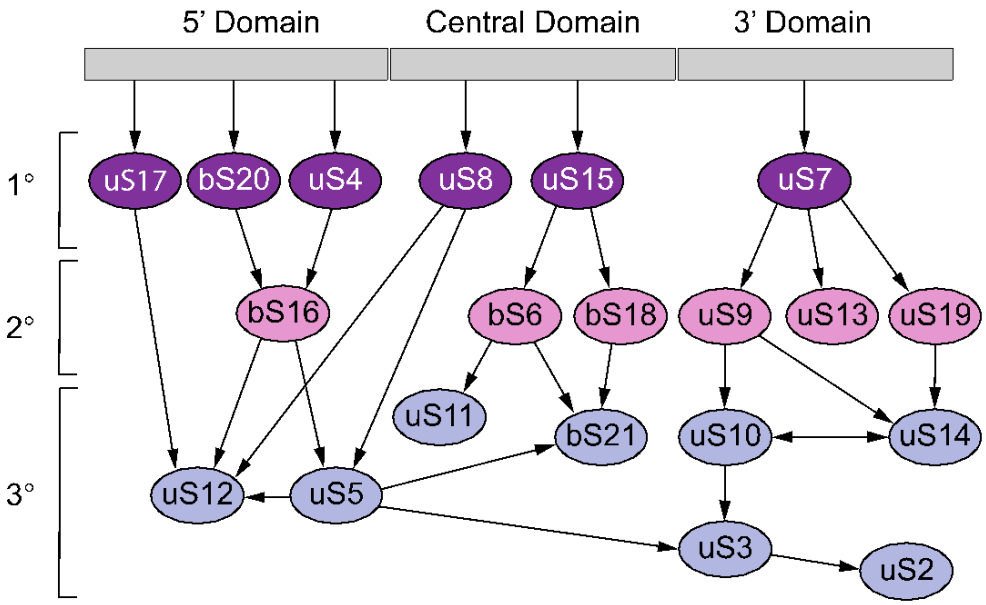

Fig 2. The 30S ribosomal subunit assembly map. Assembly of ribosomal proteins (ovals) and 16S rRNA (grey bar) based on in vitro reconstitution. Primary binding proteins (purple) bind directly to 16S rRNA in the absence of other proteins. Secondary binding proteins (pink) depend on prior binding of primary binding proteins. Tertiary binding proteins (grey-blue) require prior binding of primary and secondary binding proteins. Arrows indicate dependencies. (Figure based on Held et al., 1974).

30S subunit assembly is assumed to occur concurrently with rRNA synthesis and rRNA folding; assembly occurs via multiple parallel pathways, based on evidence from cryo-EM (Jomaa *et al.,* 2011; Chen *et al.,* 2015; Davis, 2017; Qin *et al.,* 2023; Webster *et al.,* 2023), time-resolved hydroxyl radical footprinting (Woodson, 2011; Hulscher *et al.,* 2016), and mass spectrometry (Adilakshmi *et al.,* 2008; Sashital *et al.,* 2014). This means that the order in which proteins bind differs from one assembling ribosome to the next, excluding any simple model for assembly. In addition, nucleotides contacted by the same protein are protected at different rates, indicating an induced fit mechanism in which RNA-protein intermediates refold during assembly to create binding sites for later-binding proteins. Concurrent nucleation of assembly can occur along different points of the rRNA and different rates of protection for proteins allow complexes to refold during the assembly process, indicating a versatile assembly process that is different from one ribosome to the next (Adilakshmi *et al.,* 2008). This use of multiple pathways allows for an increase in the assembly process' flexibility and allows accessory factors and rRNA modifying enzymes to assist with late-stage assembly and quality control of the subunits as they reach their mature state (Woodson, 2008).

My thesis project is part of a larger effort to identify ribosomal proteins that are critical for a major 16S rRNA folding event that must occur during 30S ribosomal subunit assembly. The purpose of this thesis was to examine a specific ribosomal protein, bS20, of the extremely thermophilic bacterium *Thermus thermophilus* (Figure 3). This protein has not been the focus of extensive research over the years. It has been found to be dispensable in mesophiles (Dabbs 1991; Baba *et al.,* 2006;

Bubunenko, Baker, & Court, 2007; Tobin *et al.,* 2010; Shoji *et al.,* 2011), however, there has yet to be published data where it has been deleted in a thermophile. The role of bS20 is still not completely understood, but research in mesophiles does show that it may participate in both assembly and function. Importantly, previous studies have also shown that bS20's abundance is reduced in a putative 30S subunit assembly intermediate that accumulates in mutants lacking the gene encoding ribosomal protein uS17 (Simitsopoulou 1999). Both bS20 and uS17 are primary binding proteins that interact extensively with the 5' domain of 16S rRNA (Wimberly *et al*., 2000).

For my thesis, I constructed a mutant of the extremely thermophilic bacterium *T. thermophilus* in which I deleted the *rpsT* gene encoding bS20 and assessed the growth characteristics of this mutant. I then compared its phenotype to that observed for a *T. thermophilus* uS17 deletion mutant, which is known to have a severe 30S subunit assembly defect. I find that loss of bS20 produces a slow-growth phenotype, consistent with a role in 30S subunit assembly. This phenotypic effect is much less severe than that caused by loss of ribosomal protein uS17. In addition, I find that the mutant is hypersensitive to streptomycin, an aminoglycoside antibiotic that induces translational misreading, suggesting a role for this protein in ribosome function after assembly is completed.

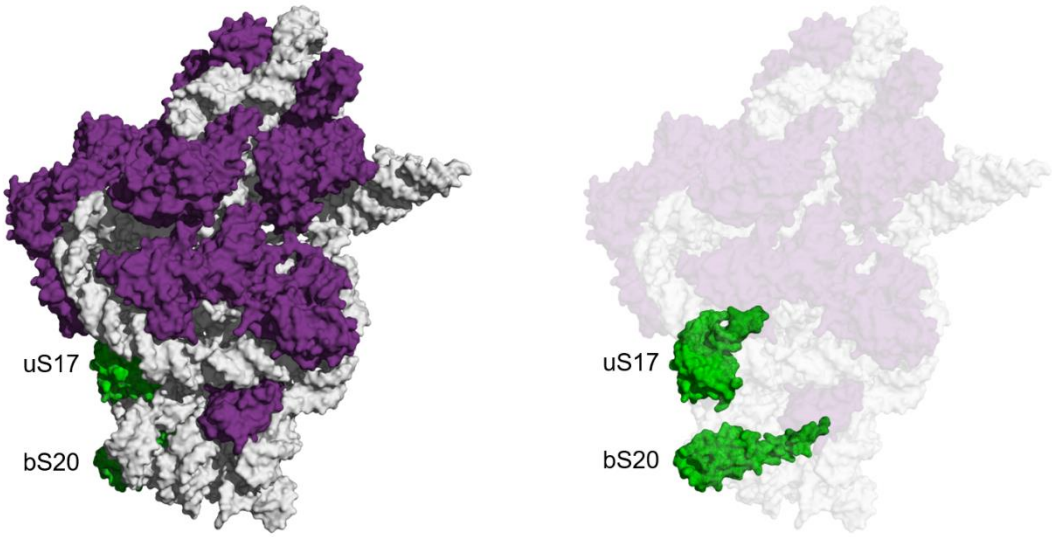

Figure 3. 30S subunit surface rendering. (Left) Surface rendering of the 30S subunit with 16S rRNA colored white, uS17 and bS20 green, and the remaining proteins violetpurple. (Right) Same surface rendering except that all but uS17 and bS20 are shown at 80% transparency to better show their interactions with the remaining 30S structure. Surface renderings generated with PyMOL using pdb entry 4y4p (Polikanov et al., 2015).

Ribosomal protein uS17

uS17 is an early assembly primary binding protein, meaning it binds directly to the 16S rRNA (Held *et al.,* 1973; Bubunenko, Baker, & Court 2007; Woodson, 2008). As shown from both chemical footprinting experiments and high-resolution ribosome crystal structures, uS17 binds to 16S rRNA helices 7 and 11 (h7 and h11, respectively) near the central junction and stabilizes a so-called 'K-turn' motif in the h11 (location seen in Figure 4). Together with primary binding protein uS4, uS17 stabilizes the 5’ domain of 16S rRNA (Ramaswamy & Woodson, 2009). While the critical uS17 interactions have not been elucidated to date, it is known that uS17 makes extensive and long-range contact with the rRNA in both the 5’ domain and central domain. Given the 5’ to 3’ directionality of transcription, it

seems most likely that uS17 binds initially to the 5’ domain then recruits the central domain in a major 16S rRNA global folding event.

This 16S rRNA folding event involves a series of RNA-RNA interactions between parts of the 5' domain and h20-h21 in the central domain (Ramaswamy & Woodson, 2009). This then creates the binding sites for a subset of other proteins, including bS20. These later protein binding events serve to stabilize this global fold of 16S rRNA. We hypothesize that during ribosome assembly, the stabilization and/or acceleration of the formation of the h21-h23 coaxial stacking interactions with the 5’ domain requires uS17 binding. With all this information, the Gregory laboratory has predicted some long-range binding interactions between the uS17 and 16S rRNA in the 5’ and central domains to be important for this folding event.

Deletion of the *rpsQ* gene, which encodes uS17, causes a severe subunit assembly deficiency that leads to a temperature-sensitive phenotype and a severe growth defect. This phenotype has been observed in several bacterial species, including the mesophile *E. coli* (Stoffler-Meilicke *et al.,* 1985; Shoji *et al.,* 2011) and the thermophile *T. thermophilus* (Simitsopoulou, Avila, & Franceschi, 1999). The Gregory laboratory has been able to recapitulate this phenotype by constructing its own uS17 knockout mutant of *T. thermophilus.* While the mutant is unable to grow at the thermophile’s normal optimal 65 °C, it is able to grow only very slowly at 55 °C. Based on sucrose density gradient sedimentation, it has become clear that the uS17 deletion strain produces a mixed population of 30S subunits and a smaller particle sedimenting at 20S. This 20S was first observed by the Simitsopoulou lab and their collaborators. 2D gel electrophoresis showed that, in

addition to the absence of uS17, ribosomal proteins uS5, uS16, and uS13 r-proteins were missing and uS4, uS8, uS15, bS18, and bS20 were significantly reduced in amounts (Simitsopoulou, Avila, & Francheschi, 1999).

When sucrose gradient sedimentation was performed by the Gregory lab at a lower Mg^{2+} concentration, multiple additional peaks were observed in the general area of the 20S particle found by Simitsopoulou, suggesting a heightened Mg^{2+} dependence and structural instability of the 20S particle. It is not known if the fully assembled 30S subunits are also less stable. Under the mutant's permissive conditions, a mixture of assembly-defective 20S particles and fully assembled 30S subunits are formed. The latter go on the join the 50S subunit and become the 70S ribosome responsible for protein synthesis. The Gregory lab's structural biologist collaborators at Brown University have solved the structure of the fully assembled uS17-minus 70S ribosome using X-ray crystallography (pdb entry 5v8i, unpublished). This structure confirms that, even with the absence of uS17, native 30S subunits do form, with only subtle changes in 16S rRNA conformation around the uS17 binding site. The current model, therefore, is that uS17 accelerates the folding process, which occurs slowly in its absence. The assembly defect is therefore primarily a kinetic one.

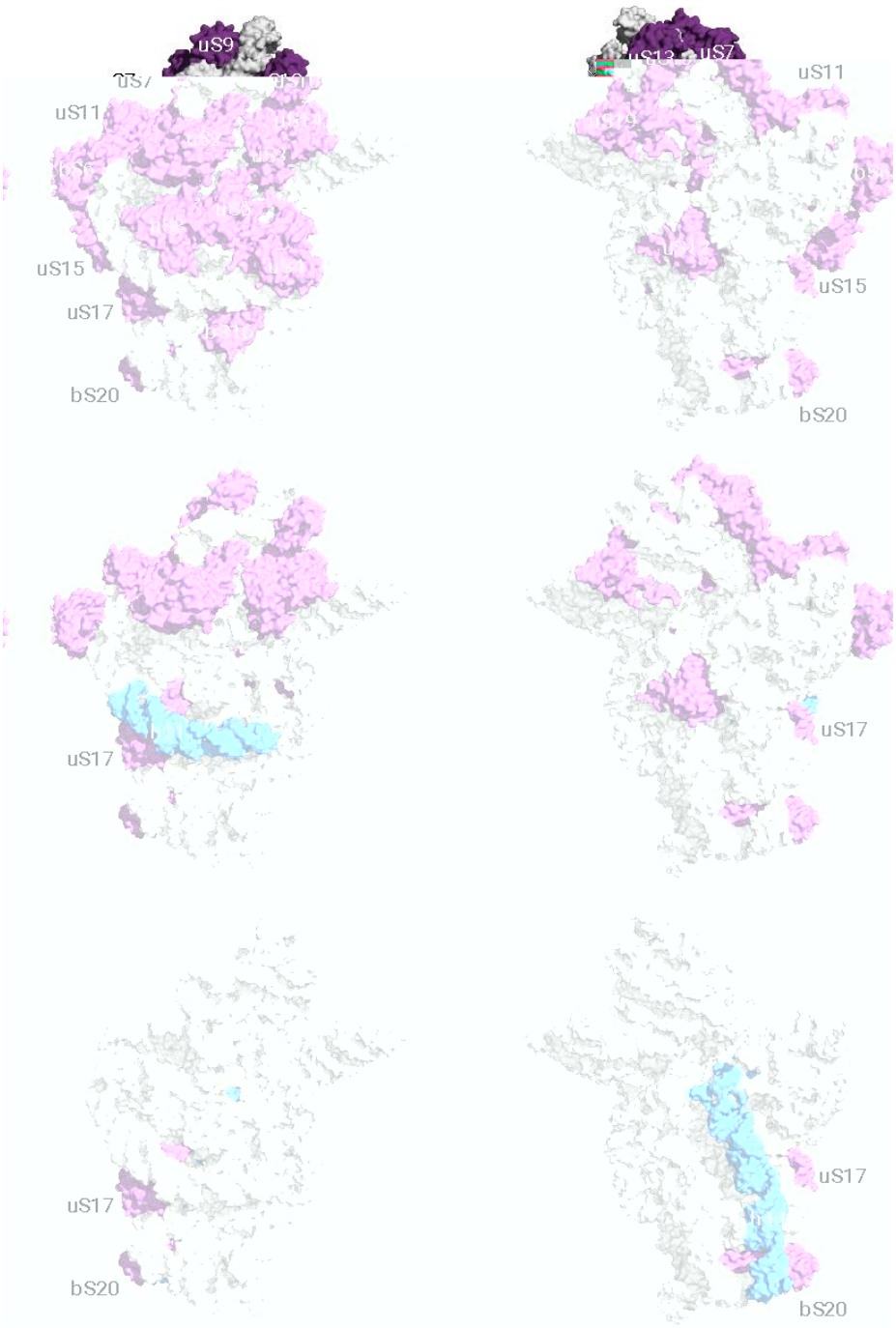

Fig 4. Surface rendering of the *T. thermophilus* 30S subunit. Shown in the context of the 70S ribosome (pdb entry 4y4p; Polikanov et al. 2015), viewed from the solvent side (left) and from the subunit interface side (right). 16S rRNA is colored white and ribosomal proteins violetpurple. (Top row) The intact 30S subunit with ribosomal proteins labeled. (Middle row) The 30S subunits with proteins absent or reduced in the uS17-minus mutant removed, and 16S rRNA helix 21 colored skyblue. (Bottom row) The 30S subunit showing only 16S rRNA and ribosomal proteins uS17 and bS20, with 16S rRNA helix 44 colored skyblue.

Ribosomal protein bS20

Adjacent to uS17 in the 30S subunit is ribosomal protein bS20, a 106 amino acid protein organized into three alpha-helices. This protein, like uS17, is a primary binding protein that interacts with the 16S rRNA 5’ domain, where it affects local rRNA conformational stability. It is also one of the proteins that is reduced in subunit assembly-defective particles that accumulate in uS17-minus mutants. As seen in the 16S rRNA tertiary structure above, uS17 and bS20 are in a similar region of the subunit. Even though they do not come in contact with each other, both have binding sites in the 16S rRNA 5' domain (Figure 5).

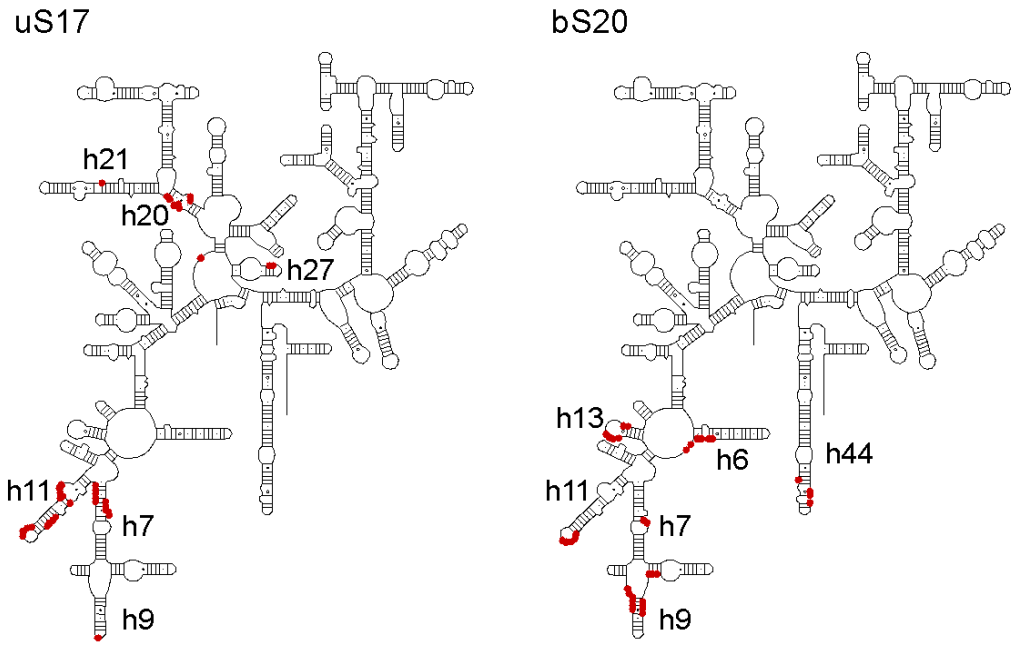

Figure 5. Binding sites for uS17 and bS20 on 16S rRNA. Secondary structure maps of *T. thermophilus* 16S rRNA (Cannone *et al*., 2002), with sites of contact with ribosomal proteins uS17 (left) or bS20 (right) indicated by red dots. Relevant helices are indicated.

In *E. coli,* the *rpsT* gene encoding bS20 has been shown to have two promoters, separated by 90 base pairs, which can both direct the synthesis of “runoff” transcripts (Mackie & Parsons, 1983). The first promoter is responsible for 10-30% total transcription of *rpsT*, with the second promoter doing the rest. The reason bS20 has these two promoters that can act independently or additively is still not fully understood but is an interesting characteristic of this ribosomal protein gene. Like many other ribosomal proteins in *E. coli,* bS20’s synthesis is regulated autogenously either posttranscriptionally or during translation. This protein is also one of the few that act as repressors, and can mediate posttranscriptional control by binding, in competition with assembling ribosomes, to their own mRNAs (Parsons, Donly, & Mackie, 1988). This allows free bS20 concentration in the cell to be used for posttranscriptional regulation and controlling translation initiation efficiency.

Interestingly, *rpsT* uses a UUG initiation codon, which is not a commonly used codon, that is important for its efficiency. Double mutations to certain residues in this codon reduce the *in vitro* translation efficiency and *in vivo* mRNA stability (Parsons, Donly, & Mackie 1988). Based on all this information, there is evidence that bS20 is capable of *in vivo* and *in vitro* regulation of its synthesis, post-transcriptionally. In contrast, little is known about *rpsT* regulation in *T. thermophilus*, though it appears to use an AUG start codon.

Research completed in *E. coli* has demonstrated that *rpsT* can be deleted and is therefore nonessential (Dabbs 1991; Baba *et al.,* 2006; Bubunenko, Baker, & Court, 2007; Shoji *et al.,* 2011). Alongside uS4 and uS17, this protein helps to stabilize the 5’ domain’s folded structure in *E. coli.* They enable the recruitment of

bS16 to the 5’ domain at the interface between uS4 and uS17-bS20 subdomains. When using three-color single molecule FRET, it has been observed that while these four proteins do not directly contact one another, their binding sites are connected by rRNA tertiary interactions (Abeysirigunawardena *et al.,* 2017). These binding sites can be seen in Figure 7. FRET data further show that a conformational change in the bS20 binding site in the 5’ domain may be required for bS16 to bind and stabilize.

Unlike uS4 and uS17, which have more extensive long-range global impacts, bS20 affects the 16S rRNA more locally (Ramaswamy & Woodson, 2009). Its long-range interactions are limited to helix h44 in the 3’ minor domain. Given that h44 is one of the last structures in 16S rRNA to be synthesized, this interaction probably occurs very late in assembly. This is why I hypothesized that a deletion mutant of *rpsT* would have a similar but less severe phenotype than that of the uS17 deletion mutant. This penultimate 16S rRNA helix is important for interaction with the 50S subunit and contains an important functional center, the decoding site, where codon recognition takes place. However, the bS20 binding site is distant from the decoding site (roughly 80 Å) suggesting that it is unlikely to directly affect this process.

While bS20 is not an essential protein, there has been an increasing interest in this protein and its effects, using the model bacteria *E. coli* and *Salmonella typhimurium* serovar *enterica* (hereafter, *S. enterica*). While bS20 deletion mutants are viable, the absence of bS20 hinders the formation of 70S ribosomes by impairing the association between the 30S and 50S subunits trying to join together (Dabbs,

1978; Gotz *et al.,* 1990). The mutants misread all three stop codons more frequently and increase tRNA suppressor efficiencies, as well as misread nonsense codons and reduce growth rate versus the wild type cells (Aulin *et al.,* 1993). Protein bS21, one of the last binding proteins during assembly, has a reduced abundance when bS20 is deleted, possibly due to impairments in the subunit's assembly. It remains unclear, however, if bS21 binding is dependent on bS20 binding, modifications that bS20 binding causes to 16S rRNA, or both (Aulin *et al.,* 1993).

Looking at bS20 in *S. enterica,* it was found that while a *rpsT* deletion mutant grew slower than wild type, it was able to maintain a rate of peptide elongation that was the same as the wild type (Tobin *et al.,* 2010). There was a reduction in mRNA binding rate and severe defects in translation initiation, due to decreased 70S ribosomes being made. Both defects could be partially overcome by extending their incubation time with mRNA, fMet-tRNA^{fMet}, and initiation factors (Tobin e*t al.,* 2010). This points to the absence of bS20 disrupting the 30S subunit's structural integrity.

Despite all the research described above, bS20's role in 30S subunit assembly is still not fully known. Research has been focused on this protein in mesophiles like *E. coli* and *Salmonella.* There has been no research done in other types of bacteria, like thermophiles for example. While it is known that bS20 is nonessential in mesophiles and causes a variety of effects, it cannot be assumed that these trends would be similar in other bacteria. The ribosomes of thermophiles tend to be more robust, meaning that the deletion of bS20 could have less severe effects, no effects, or even different effects. One point of my thesis work was to assess the

essentiality of bS20 in the thermophile *T. thermophilus*. I also sought to compare the phenotype of a bS20 knockout mutant to that of a mutant lacking the important assembly protein uS17.

Antibiotics and ribosome assembly

Over 50% of antibiotics target the ribosome and obstruct translation. This makes sense as ribosomes have a very large and complicated structure, which offers many binding sites for antibiotics. More recent studies have implicated antibiotics in inhibiting ribosome assembly. This leads me to the hypothesis that ribosomal mutants with assembly defects might be hypersensitive to antibiotic inhibitors of protein synthesis.

Antibiotics bind to both the large and small subunit of the ribosome, usually in sites with a lot of activity and that are predominantly, if not exclusively, rRNA. Aminoglycosides, macrolides, and thiopeptides are the classes of antibiotics that target the 30S subunit, 50S subunit, and 70S ribosome, respectively. Aminoglycosides work by binding directly to the 30S subunit's 16S rRNA, (Cundliffe & Demain 2010). Macrolides, which target the large ribosomal subunit, have also been found to disrupt the assembly of the 30S subunit (Siidak e*t al.,* 2009; Siidak *et al.,* 2011). A major target is the peptidyl transferase center, or PTC, in the large subunit (Vasques, 1979; Cundliffe, 1981; Polacek & Mankin, 2005; Brown & Wright, 2016). The most common site targeted in the smaller subunit is the A site decoding region. Here aminoglycosides can interfere with the aminoacyl-tRNA·EF-TU·GTP selection (D'Costa *et al.,* 2011).

There are protein synthesis inhibitors that are known to also inhibit ribosome assembly; it has been found that inhibition of translation generally causes an imbalance between rRNA and r-protein production, which in turn causes assembly defects (Takebe *et al.,* 1985). However, this is an indirect consequence wherein the inhibition of protein synthesis causes a decrease in ribosomal protein production and consequently an increase in rRNA production that causes an imbalance of available rRNA and r-proteins (Siidak *et al.,* 2009). There were no defined assembly intermediates or dead-end particles found in sucrose gradients, which would be expected if there was a direct binding of drugs to the pre-assembled ribosome particles. Therefore, it is the inhibition of ribosomal protein synthesis that indirectly inhibits assembly.

In this thesis, I examined a hypothesis that an assembly defect associated with deletion of *rpsT* should lead to hypersensitivity to antibiotic inhibitors of protein synthesis. This was unable to be done with the uS17 deletion mutant due to its extreme growth defect. Based on the information above, a variety of antibiotics were chosen. This includes antibiotics that inhibit protein synthesis by binding to either the 30S subunit or the 50S subunit.

Thermus thermophilus **as a model system**

T. thermophilus is an extremely thermophilic, obligately aerobic, gram-negative, nonsporulating rod, belonging to the *Deinococcus-Thermus* phylum in the Bacterial domain, and was first discovered in a Japanese hot spring (Oshima & Imahori, 1974). It can be found in domestic hot water heaters as well as natural

thermal habitats (Brock & Freeze 1969; Kristjansson & Alfredsson, 1983). As a thermophile, it has an optimal growth temperature of 65-72 °C with the ability to grow as low as 47 °C and as high as 85 °C (Cava, Hidalgo, & Berenguer, 2009). Thermophiles often have higher G+C contents than their mesophile counterparts, with *T. thermophilus* having a 69% G+C content (Henne *et al.*, 2004).

While there are multiple *T. thermophilus* strains that can be used experimentally, the Gregory laboratory primarily uses strain HB27, which is the most widely used strain. It has both a main chromosome and a megaplasmid, denoted pTT27 (Henne *et al.,* 2004). It is a good model organism due to its natural competence for transformation with plasmid or genomic DNA, allowing gene replacement by homologous recombination. This allows for easy genetic manipulation of the bacterium without needing to disrupt the cell membrane using electroporation, or incubation in calcium chloride used in artificial transformation (Koyama *et al.,* 1998; Cava, Hidalgo, Berenguer, 2009). Another characteristic facilitating ribosomal genetics is the presence of only two copies of each rRNA gene. This allows for production of homogenous ribosome populations by either gene conversion or constructing strains with a deletion of one rRNA gene copy.

Lastly, ribosomes from thermophiles are easier to crystalize than those of other bacteria. Many X-ray crystal structures of the *T. thermophilus* ribosome have been solved. These include just the 30S subunit, just the 50S subunit, the full 70S assembled ribosome, and with various other elements attached (Trakhanov *et al.,* 1987; Trakhanov *et al.,* 1989; Cate *et al.,* 1999; Schluenzen *et al.,* 2000; Wimberly *et al.,* 2000; Yusupov *et al.,* 2001). The current highest resolution for the *T.*

thermophilus 70S structure is 2.4 Å and was solved by X-ray diffraction (Polikanov *et al.,* 2015). These structures allow researchers to design and predict the effects of mutations on ribosome structure, function, and assembly.

CHAPTER 2

Methodology

Bacterial strains and growth conditions

All *E. coli* strains used in this study were derived from strain K12 and were grown in standard LB or SOC medium. All *T. thermophilus* strains used in this study were derived from the HB27 strain (ATCC BAA-163; Oshima & Imahori, 1974). These strains were grown in Thermus Enhanced Medium (TEM, ATCC Medium 1598). TEM plates were solidified with 1.8% (w/v) Difco agar. TEM was made using (per 1 L): 0.2 g $MgCl_2$•$6H_2O$, 0.04 g $CaSO_4$•$2H_2O$, 0.154 g Na_3Citrate•$2H_2O$, 2.5 g yeast extract, 2.5 g tryptone, 900 mL deionized H_2O, 0.5 mL 0.01 M Fe citrate, 0.5 mL Trace Element Solution (per 1 L: 1.97 g Na_3Citrate•$2H_2O$, 0.1 g $FeCl_2$•$4H_2O$, 0.05 g $MnCl_2$•$4H_2O$, 0.03 mg $CoCl_2$•$2H_2O$, 0.005 g $CuCl_2$•$2H_2O$, 0.005 g Na_2MoO_4•$2H_2O$, 0.002 g H_3BO_3, and 0.002 g $NiCl_2$•$6H_2O$). The mixture was autoclaved alongside 100 mL phosphate buffer (per 1 L: 5.44 g KH_2PO_4, 17 g Na_2HPO_4 pH 7.2) which was added to the mixture post-autoclave. Liquid culture was made same as the solid media, without the agar. All bacterial stocks were stored in glycerol (25% w/v) at -80 °C. All gDNA and plasmid DNA were stored at -20 °C.

Enzymes and reagents

Enzymes were purchased from New England Biolabs (NEB; Ipswich, MA) and were used according to the manufacturer's specifications. OneTaq DNA

Polymerase (NEB catalog number M0482L) was used for PCR amplification for Sanger sequencing and Diagnostic PCR. DNA Clean and Concentrator Kit (catalog number D4034) from Zymo Research (Irvine, CA) was used to purify PCR products and restriction fragments to be used for cloning. *E. coli* plasmids were purified using Zymo Research ZR Plasmid Miniprep Kit (catalog number D4015). Lastly, genomic DNA (gDNA) from *T. thermophilus* were purified using the Wizard Genomic DNA Kit (cat number A2920) from Promega (Madison, WI).

Oligonucleotides

All oligonucleotide primers used in this study were purchased from Integrated DNA Technologies (IDT, Coralville, IA) and are listed in Table 1 below. Once received, the lyophilized primers were dissolved in TE buffer 100 µM concentration, and 10 µM working stocks were made by dilution in water.

Q5 mutagenesis

Q5 mutagenesis was used for creating mutants of interest. The primers were used to incorporate the mutation during amplification of the plasmid using the Q5 Hot Start High-Fidelity DNA Polymerase (NEB #M0492). A KLD reaction, which ligates the PCR product and removes the template, was then performed using NEB's KLD Enzyme Mix Kit. The KLD reaction was incubated at room temperature for 5 minutes before being used to transform *E. coli* competent cells taken directly from the -80 ˚C freezer and thawed on ice.

DNA assembly and molecular cloning

The target sequence of interest (insert) and vector were digested using specific enzymes (NEB), and the vector was further treated with rSAP (recombinant shrimp alkaline phosphatase) from NEB (catalog number M0371S), in CutSmart Buffer. Digests were incubated at 37 °C for 2 hours before being purified with Zymo PCR Cleanup Kit (D4034) and electrophoresed on a 1% agarose gel. Ligation reactions with 1:1 and 10:1 insert: vector ratios were prepared with ligase buffer and T4 DNA ligase. Ligations were incubated at room temperature for one hour and used to transform *E. coli* competent cells (NEB5 α cells for a pUC18-derived plasmids and PIR1 cells for plasmids replicating from the R6Kγ replication origin). Transformations were performed and final plasmid selected/verified as stated in the Q5 mutagenesis section.

DNA sequencing

PCR products were sequenced by Sanger sequencing by the RI-INBRE Core Facility, housed in Avedisian Hall.

Transformation of competent *E. coli*

Frozen competent NEB5α *E. coli* cells (genotype *fhuA2Δ(argF-lacZ) U169 phoA glnV44 Φ80Δ(lacZ)M15 gyrA96 recA1 relA1 endA1 thi-1 hsdR17*; NEB catalog number C2987H) were transformed with pUC18-derived plasmids according to the manufacturer's protocol. Transformations were incubated on ice for 30 minutes, followed by being heat shocked in an Eppendorf ThermoStat at 42 °C for 30 seconds before being transferred back onto ice for at least 30 seconds. SOC

(Super Optimal broth with Catabolite repression) was added to the transformations and placed in a shaking ThermoStat to incubate for an hour at 37 °C.

The transformations were selected on LB plates containing 300 μg/ml ampicillin (LB Amp300 plates) and incubated at 37 °C. Single colonies were streaked for single colonies on the same medium and incubated at 37 °C. Purified colonies were used to inoculate 5 ml LB medium and grown overnight with shake at 37 °C. 3 ml of saturated culture were used for plasmid preparations using the Zymo miniprep classic kit. 0.8 ml of culture was archived as glycerol stocks.

The same protocol was used to transform One Shot frozen PIR1 competent *E. coli* cells (Invitrogen catalog number C101010; genotype F⁻Δ*lac169rpoS*(*AM*) *robA1 creC510hsdR514 endA recA1 uidA*(Δ*MluI*)::*pir-116*) with plasmids replicating from the R6Kγ origin, except those selections were performed on LB plates containing 50 μg/ml hygromycin B.

Transformation of *Thermus thermophilus*

Thermus thermophilus strain HB27 or mutant derivatives were streaked for single colonies from a frozen glycerol stock onto a TEM plate, with appropriate antibiotic if necessary. A 125 mL baffled flask of 10 mL TEM was inoculated with a single colony and grown overnight with aeration at 65 °C until saturated. It was then diluted 1:100 into 20 mL of prewarmed TEM with 0.4 mM $CaCl_2$ and 0.4 mM Mg_2Cl in a 250 mL baffled flask. It was incubated with aeration at 65 °C for 2 hours. In clean 125 mL baffled flasks 5mL of culture and the DNA of interest was added and incubated for 4 hours at 65 °C with aeration. The transformations were plated

on TEM with appropriate antibiotic if necessary and placed in a 65 °C standing incubator for several days until colonies appeared and could be re-streaked for single colonies. Single colonies were picked, and 10 mL TEM liquid inoculated in a 125 mL baffled flask with aeration in a shaking incubator at 65 °C. When saturated, glycerol stocks were made, and the remaining culture was harvested for genomic DNA preps. If antibiotics were not able to be used to screen and select for the desired transformants, this was determined using colony PCR, gel electrophoresis, and Sanger sequencing.

Processing of transformants

Transformations were then plated on LB medium containing appropriate antibiotic at 37 °C overnight. From there the samples were re-streaked on solid LB media, single colonies grown in liquid LB media, and plasmid DNA prepared using the Zymo Research Classic DNA Miniprep Kit (catalog number D4015). Diagnostic PCR was run on the samples amplifying different regions of the fragment (UHR & htk, DHR & htk, UHR & DHR). The samples matching the expected length when run on a gel were sent for Sanger sequencing.

Growth rate measurements

Single colonies grown on TEM plates were used to inoculate 20 mL of TEM liquid media with a minimum of three replicates performed for each genotype

(including wild type *T. thermophilus* HB27 for comparison). Cultures were grown overnight to saturation before being diluted in a baffled culture flask with 225 mL TEM for a starting OD_{600} ~0.08. The cultures were shaken at 65 °C (55 °C for the uS17 mutant). OD_{600} readings were taken every half hour until OD_{600} read 0.80 was reached (beginning of stationary phase). The readings were entered into Excel and graphed using the Chart Wizard on the menu bar (including "display equation" and "display R-squared value"), and doubling time was calculated using the equation: log2/slope (or 0.301/slope). The mean of the replicates was calculated and compared to that of the wild type growth rate measurements (see section about statistics below).

Antibiotic disc diffusion assays

Antibiotics were dissolved in the appropriate solvent to 10 µg/µL. From there 10 µL of each antibiotic was added to sterilized 6 mm filter paper discs, which were manipulated using ethanol-and-flame-sterilized forceps. Each disc contained a final amount of antibiotic of 100 µg. The only exception was ampicillin, which has an effective minimum inhibitory concentration, and only had 1 µL of the antibiotic to make the disc amount 10 µg (Peechakara *et al.,* 2023). The discs were allowed to air dry at room temperature in a sterile, empty petri dish before being moved into 1.5 mL Eppendorf tubes and stored in the -20 °C freezer. The bacterial samples to be tested were grown overnight at 65 °C in TEM. Once saturated, 100 µL of the samples were spread-plated on TEM plates and left to dry at room temperature. Once dry, sterilized forceps were used to place antibiotic discs, 2-3 different

antibiotic discs per plate. These were then placed in the 65 °C standing incubator to grow. Once the cultures were grown, a ruler was used to measure the diameter of the zone of inhibition (area around the disc where colonies were unable to grow in the presence of the antibiotic). This experiment was done in triplicate per sample with each antibiotic.

Statistical analysis

Statistical analyses were performed on the antibiotic disc diffusion assay data and the growth rate data (wild type versus complement). All tests were performed using Excel's T-Test functions. Barlett's test for homogeneity of variance between the wild type and complement growth rates was performed using the Stat Trek website. Information about the Kruskal Wallis and Welch's T-tests were looked at using the Statistics Kingdom website. Lastly, standard errors were calculated using a free online calculator website called Good Calculators.

16S rRNA secondary structure maps

Schematic 16S rRNA secondary maps were downloaded from the Comparative RNA Website (https://crw-site.chemistry.gatech.edu; Cannone et al. 2002). A postscript file (s.16.b.T.thermophilus2.schem.ps) was modified in Adobe Illustrator 2020, removing extraneous text. Line thickness (representing the phosphodiester backbone) was increased to 1pt to enhance visibility in the final figure. The image was exported from Illustrator as a .png file and imported into Microsoft PowerPoint

version 16.06 and annotated. The final figure was exported as a .pdf file and embedded in the text of the thesis.

30S subunit reconstruction map

The 30S reconstitution map figure was generated in Adobe Illustrator 2020, exported as a .pdf file, and embedded in the text of the thesis.

Ribosome structure images

All ribosome structure files were downloaded from the Protein Data Bank (https://www.rcsb.org). Images were generated with PyMOL Molecular Graphics System Version 2.2.0 (Schrödinger LLC, and DeLano, W (2020)) using PDB entry 4y4p.cif, the 2.5 Å resolution crystal structure of the *T. thermophilus* 70S ribosome (Polikanov et al., 2015). Surface renderings were performed using the default probe radius setting of 1.4 Å. Individual surfaces were created for 16S rRNA and individual ribosomal proteins. Semi-transparent surfaces were generated using a transparency setting of 0.8. Ray-traced images at 600 dpi were exported as .png files, then imported into Microsoft PowerPoint and annotated. Final figures were then exported from Microsoft PowerPoint as .pdf files and embedded in the text of the thesis. PyMOL scripts are available upon request.

Ribosome structure distance measurements

For distance measurements, cif structure files were obtained from the Protein Data Bank (https://www.rcsb.org) and opened in PyMOL. The ribosome structure

was shown in stick format, and distances were measured using the PyMOL "wizard measurement" tool, with a cutoff distance of 3.0 Ångstrom. Individual atom pairs were manually picked, and distance output was copied and pasted into a table in a .docx file. Atom identifiers are in standard pdb format. In figures, relevant residues are shown in stick format and h-bonds, or ionic bonds are shown as dashed lines generated using the distance command. Ray-traced images at 600 dpi were exported as .png files. Final figures were made using Microsoft PowerPoint, exported as .pdf files and embedded in the text of the thesis.

Plasmid maps

Maps were generated using SnapGene Viewer version 7.0.1 (Dotmatics; www.snapgene.com).

Table 1. Oligonucleotides used in this study.

Oligonucleotide	**Sequence (5'→3')**
M13(-47)	CGCCAGGGTTTTCCCAGTCACGAC
M13_Reverse	CAGGAAACAGCTATGAC
bgaA_seq_rev1	CACGCGCACGTAGGAAAGTCC
*htk*_seq_fwd1	ATGAAAGGACCAATAATAATGACTAGAGAAGAAAGAATG
*htk*_seq_rev1	TCAAAATGGTATGCGTTTTGACACATCCACTATATATCC
HB27_rpsT_out_f1	GATGAGGACCACCTTGTGGCCGAG
HB27_rpsT_out_r1	AGGAGGGGACCTTCCGCTTC
HB27_rpsT_UHR_f1	CCTGCAGGTCGACTCTAGAGCATGTGCCCAAGTATACTTAGGC
HB27_rpsT_UHR_r1	GTCCTTTCATCGTTCTCCCCTTTGGCCC
HB27_rpsT_htk_f1	GGGGAGAACGATGAAAGGACCAATAATAATGAC
HB27_rpsT_htk_r1	TACGCCCTCCTCAAAATGGTATGCGTTTTG
HB27_rpsT_DHR_f1	ACCATTTTGAGGAGGGCGTATGGGCAAG
HB27_rpsT_DHR_r1	ATTCGAGCTCGGTACCCGGGTACGGCGCCTTCCTCGGA
rpsT-*thx*_PstI_f1	GTGATACTGCAGGGTGTGCTACACT
rpsT-*thx*_XbaI_r1	GGAAGCTCTAGAAGGAGGCCGAATAGCCTA

Table 2. Plasmids used in this study.

Plasmid	Description
pUC18	Ampicillin resistant (AmpR), *E. coli* cloning vector
pSAD1	*E. coli-T. thermophilus* shuttle vector with hygromycin B resistance (*hph),* β-galactosidase, *(bgaA)* genes
pUC18-rpsT-htk (pBML26.6)	pUC18 with *rpsT* gene replaced with kanamycin-adenyltransferase (*htk)* and upstream and downstream homology regions (UHR and DHR, respectively).
pSAD-bS20-Thx (pBML55.7)	pSAD1 with *rpsT-thx* operon cloned between the *hph* and *bgaA* genes using PstI and XbaI restriction sites.

Table 3. Bacterial strains used in this study (Eco, *E. coli*; Tth, *T. thermophilus*).

Strain	Species	Genotype	Source
PIR1	Eco	F-Δ*lac169 rpoS(Am)robA1 creC510 hsdR 514 endA recA1 uidA (*ΔMluI):pir-116	ThermoFisher Scientific
NEB5α	Eco	*fhuA2*(*argF-lacZ*)U169 *phoA glnV44* φ80 (*lacZ*) M15 *gyrA96 recA1 relA1 endA1 thi-1 hsdR17*	New England Biolabs
HB27	Tth	Wild type	ATCC
JQ144	Tth	HB27 Δ*rpsQ*	Gregory Lab Collection
BML43-45	Tth	HB27 Δ*rpsT*::*htk*	Gene replacement of *rpsT* using pUC18-rpsT-htk
BML117	Tth	Δ*rpsT*::*htk*/ pSAD-bS20-Thx	Transformation of BML43 with pSAD-bS20-Thx
BML118	Tth	Δ *rpsT*::*htk*/ pSAD	Transformation of BML43 with pSAD1 empty vector
BML123	Tth	Δ *rpsT*::*htk*/ pSAD-bS20-Thx	Transformation of BML43 with pSAD-bS20-Thx
BML125	Tth	HB27/ pSAD	Transformation of HB27 with pSAD1 empty vector
BML 127	Tth	HB27/ pSAD-bS20-Thx	Transformation of HB27 with pSAD-bS20-Thx

CHAPTER 3

Findings

The ribosomal protein, bS20, is a conserved bacterial 30S primary non-essential binding protein that plays a role in the assembly of the 30S subunit (Held *et al.,* 1974). Deletion of the *rpsT* gene encoding bS20 in mesophiles leads to a severe growth deficiency and a significant decrease in the amount of 70S ribosomes being assembled (Dabbs, 1978; Gotz *et al.,* 1989). To date, there are no published data indicating that bS20 can be removed from a thermophile's ribosome. Therefore, to test the phenotypes found by other labs in mesophiles, I created a *rpsT* knockout strain in *T. thermophilus*, which will be used to examine the role of bS20 in ribosomal 30S subunit assembly and its phenotype.

Construction of Δ*rpsT::htk* bS20-minus mutant

To delete the *rpsT* gene, I constructed a plasmid, pUC18-rpsT-htk (pBML26.6), designed using the NEBuilder online tool (https://nebuilder.neb.com/#!/). This plasmid construct consists of the pUC18 cloning vector, upstream and downstream homology regions (UHR and DHR) flanking the *rpsT* locus, and the *htk* gene encoding a thermostable kanamycin-adenyltransferase (Figure 6). The UHR and DHR, generated by PCR (see Methodology), were 466 bp and 479 bp in length, respectively, providing sufficient extents of sequence homology for efficient homologous recombination. The UHR was amplified using primers (HB27_rpsT_UHR_f1 and HB27_rpsT_UHR_r1) and the DHR was amplified

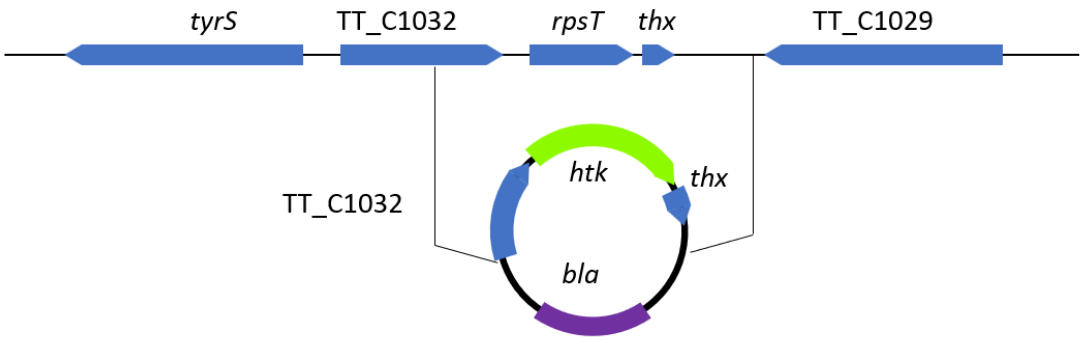

Figure 6. Schematic used to replace the bS20 encoding gene, *rpsT*. The gene *rpsT* was replaced with the highly thermostable kanamycin adenyltransferase gene, *htk.* The horizontal line at the top of the figure shows the operon that encodes *rpsT.* Below the line is a representation of the plasmid used. In green is the *htk* gene that replaced the *rpsT* gene. In blue is the upper and downstream homologous regions that were also incorporated into the plasmid to allow for homologous recombination, as shown by the vertical arrows. The *thx* gene was included in the plasmid to ensure it was not deleted alongside *rpsT,* which would have further complicated any findings as the source of said findings could be due to either *rpsT* or *thx.*

using primers (HB27_rpsT_DHR_f1 and HB27_rpsT_DHR_r1). The *htk* gene was amplified using primers HB27_rpsT_htk_f1 and HB27_rpsT_htk_f1, producing a 762 bp product. The BamHI-digested pUC18 vector backbone, DHR, UHR, and *htk* fragments were combined using Gibson Assembly. The *rpsT* coding sequence was replaced with *htk* in a one-to-one exchange of start and stop codons. Thus, the *htk* coding sequence uses the transcription and translation elements of *rpsT*.

The resulting plasmid (Figure 7) was used to transform NEB5α *E. coli* cells, and its structure was confirmed by restriction digestion and Sanger sequencing (using primers M13(-47) and M13_reverse). Once the correct plasmid was confirmed, it was used to transform *T. thermophilus* HB27, selecting kanamycin resistance.

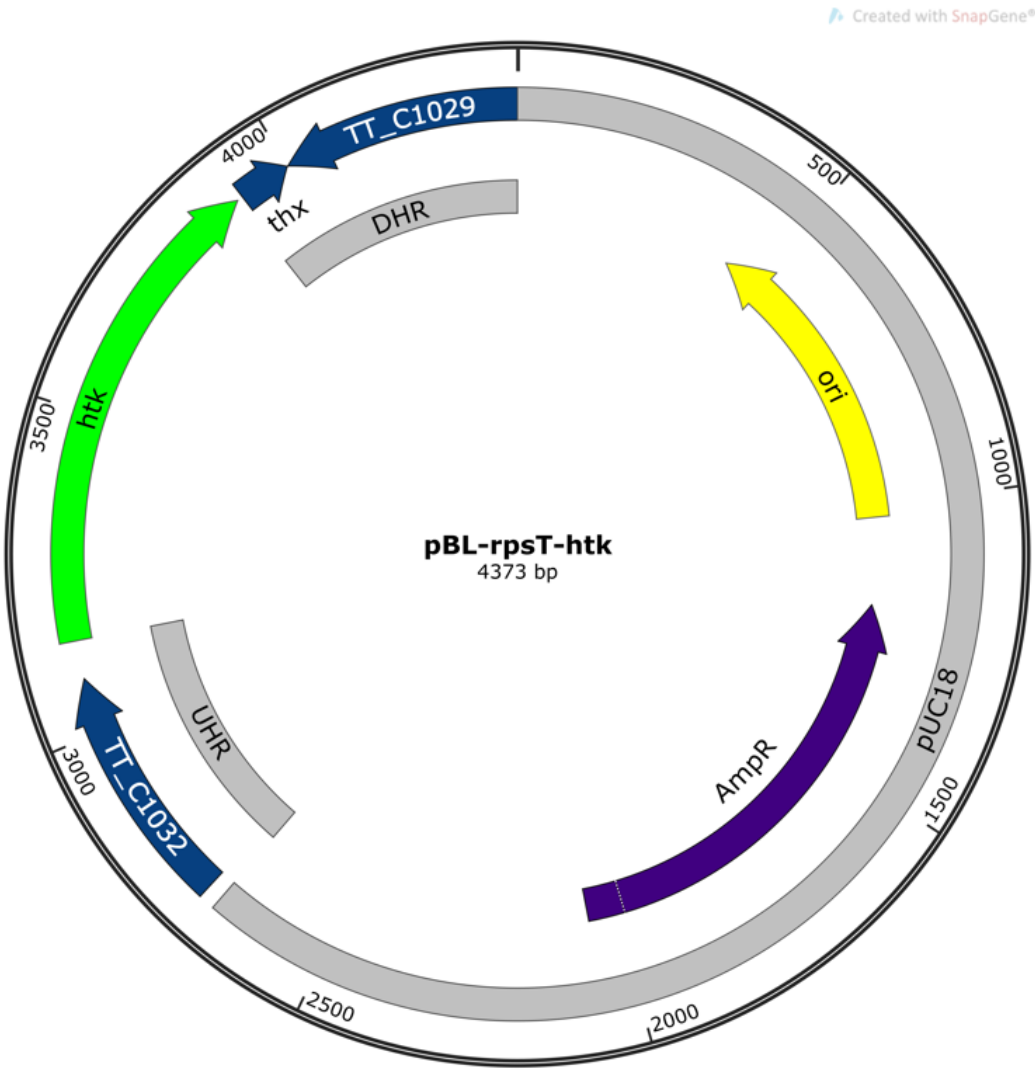

Figure 7. Plasmid construct of the *rpsT* deletion mutant (Δ*rpsT*::*htk).* The plasmid pUC18 with *rpsT* gene is replaced with kanamycin-adenyltransferase (*htk)* and upstream homology region (UHR) and downstream homology region (DHR).

As pUC18 does not replicate in *T. thermophilus*, kanamycin resistance can only result from either insertion of the entire plasmid into the chromosome by a single crossover or by exchange of the mutant and wild-type *rpsT* loci by double cross-over. A double cross-over event resulted in replacement of the native *rpsT* locus with the deletion. This general strategy for construction of knockout mutants of *T. thermophilus* has been described by my advisor for a number of genes, including *rpmA* (Cameron et al., 2004), *rrlB* (Moshupanee *et al*., 2008), *rrsA* (Gregory and Dahlberg, 2009), *ksgA* (Demirci *et al.*, 2009), *rsmG* (Gregory *et al*., 2009), *rrsB* (Carr *et al.*, 2015), *thx* (Dao *et al*., 2015) and *rlmN* (Alexandrova *et al*., 2024).

Immediately downstream of *rpsT* is *thx*, encoding ribosomal protein Thx, a small 26 aa peptide that is specific to members of the Deinococcus-Thermus phylum (Leontiadou *et al*., 2001), though it has homology to plastid-specific ribosomal protein PSRP4 (Yamaguchi *et al*., 2004). In contrast to the proximity of these two genes, their encoded ribosomal proteins are located at opposite ends of the 30S subunit (Brodersen *et al.,* 2002). Thx is dispensable in *T. thermophilus* (Dao *et al.*, 2015) and a mutant lacking it shows no growth defect (S. Gregory, unpublished observation).

Several putative knockout mutants were purified by restreaking, grown in liquid medium and archived. Putative mutants grew noticeably slower than wild type, but did not display a temperature-sensitive phenotype, in contrast to the *rpsQ* mutant lacking uS17 (designated JQ144). After purification by serial restreaking, colonies were used to inoculate liquid medium, grown to saturation, archived as glycerol stocks, and stored at -80 °C. These cultures were also used to prepare gDNA,

which in turn was used to confirm the presence of the knockout allele by diagnostic PCR.

The presence of the gene knockout was confirmed by diagnostic PCR using primer pair HB27_rpsT_out_f1 and HB27_rpsT_out_r1. These primers bind outside the region of homology used for recombination and gene replacement. Further, they are expected to amplify both the mutant and wild type *rpsT-thx* region. The expected product for wild type is 1645 bp, while that for the mutant locus is 2086 bp. As shown in Figure 10, electrophoresis of PCR products clearly indicates that the strains BML43, BML44, and BL45 all contain the knockout allele and lack an intact *rpsT* coding sequence (Figure 8). All three were sequenced (using primers *htk*_seq_fwd1 and *htk*_seq_rev1) and confirmed to have the knockout. BML43 was used for all further testing.

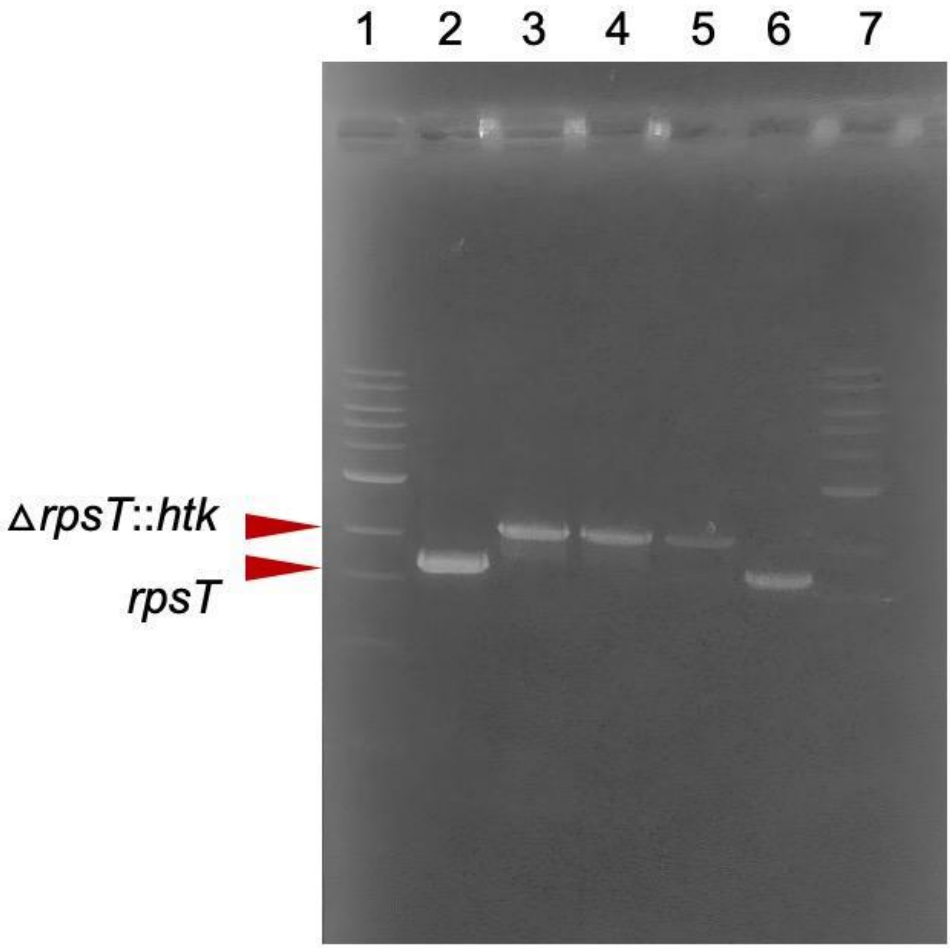

Figure 8. Diagnostic PCR to confirm deletion of *rpsT*. Lanes 1 and 7, 1 kb DNA ladder; lanes 2 and 6, PCR product from wild type *T. thermophilus* gDNA; lanes 3, 4, and 5, PCR products from three independent Δ*rpsT*::*htk* deletion mutants. The primers used were HB27_rpsT_out_f1 and HB27_rpsT_out_r1. The expected length for the wild type control is 1645 bp and the Δ*rpsT*::*htk* deletion mutants had an expected length of 2086 bp, which are confirmed in the gel above.

Complementation by plasmid expression of bS20

To demonstrate definitively that the phenotype of the *T. thermophilus ΔrpsT::htk* mutant was in fact due to the loss of bS20, I constructed a bS20 expression plasmid (Figure 9). This was based on the *E. coli-T. thermophilus* shuttle plasmid pSAD1, developed by the Gregory laboratory (Carr et al., 2015). This plasmid has both the R6Kγ replication origin and the replication origin and the *repA* gene from the *T. thermophilus* cryptic plasmid pTT8. It also contains the *hph* gene, encoding a thermostable hygromycin B phosphotransferase, driven by the strong *slpA* promoter. The *hph* coding sequence also contains the *bgaA* gene from *T. thermophilus* strain IB-21, encoding a thermostable β-galactosidase. Both genes are transcribed as part of a synthetic operon and are separated by a multiple cloning site for insertion of genes for expression. Expression of the *bgaA* gene can be easily assayed using the histochemical stain X-gal or the chomogenic substrate *p*-nitrophenyl-β-D-galactoside.

The *rpsT-thx* coding sequences were inserted as a PstI-XbaI fragment into pSAD1 between the *hph* and *bgaA* genes using primers rpsT-thx_PstI_f1 and rpsT-thx_XbaI_r1. The resulting plasmid was transformed into PIR1 *E. coli* competent cells and confirmed by gel electrophoresis (expected PCR product ~500 bp). The sequence was confirmed by Sanger sequencing using primer bgaA_seq_rev1 and designated pSAD-bS20-Thx. This plasmid was used to transform wild type *T. thermophilus* HB27 and the Δ*rpsT::htk* mutant BML43. Transformants were selected for hygromycin B resistance.

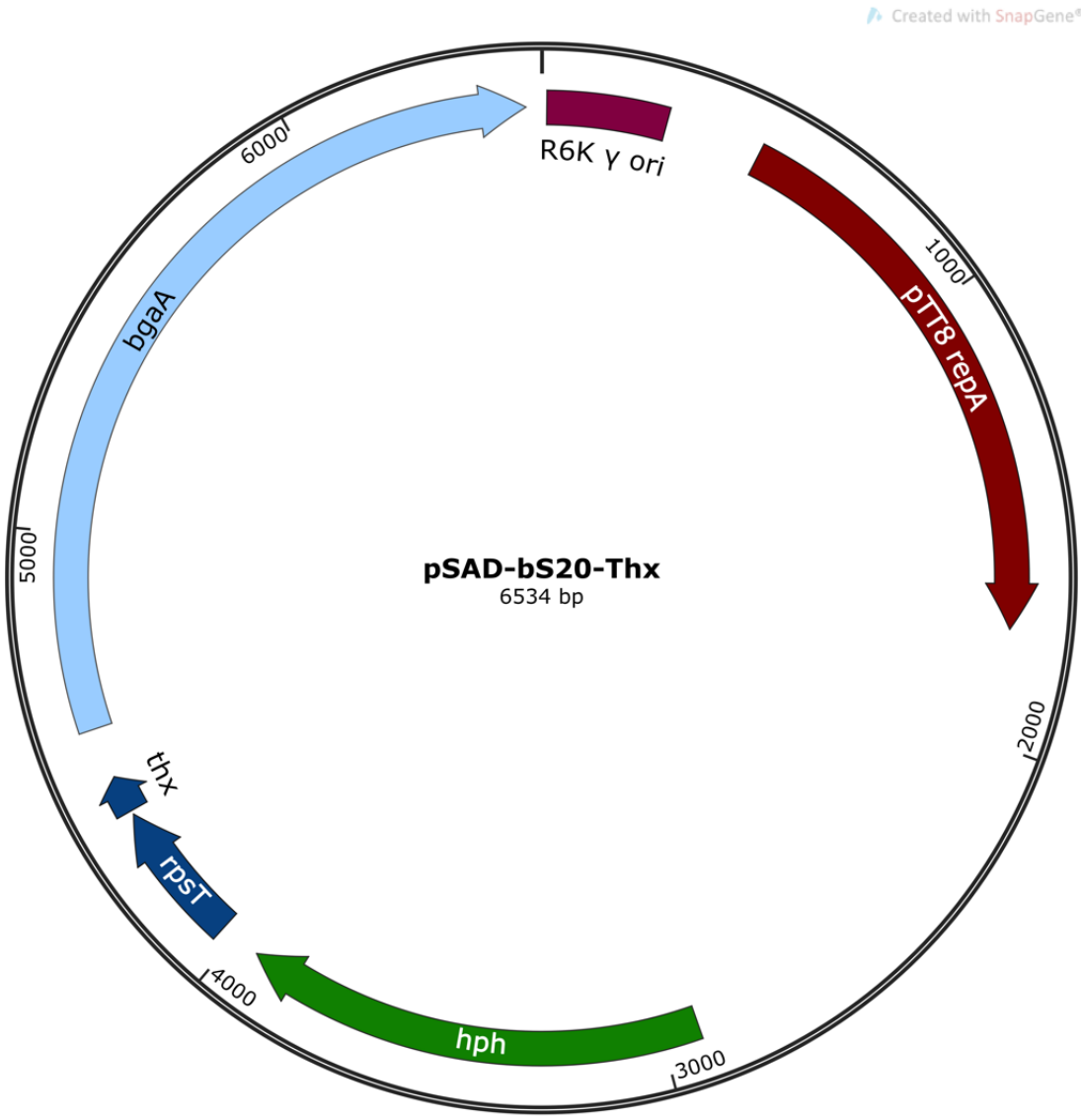

Figure 9. Plasmid construct of the bS20 expression plasmid. Plasmid pSAD-bS20-Thx with *rpsT-thx* operon cloned between the *hph* and *bgaA* genes using PstI and XbaI restriction sites.

Growth phenotype of the *ΔrpsT::htk* bS20-minus mutant

Based on previously published work, deletions of *rpsT* in other bacteria cause slower growth rates. As growth rate reflects protein synthesis capacity, this serves as a proxy for the sum total of ribosomal subunit assembly and protein synthesis activity of assembled ribosomes. I therefore performed growth rate measurements of my *rpsT* deletion mutant. This was performed in triplicate to validate observed results.

For comparison, I performed growth rates on wild type *T. thermophilus* (HB27), my bS20 knockout (BML43), and my bS20 knockout mutant with a bS20 expression plasmid (BML117) at 65 °C. I was unable to use the uS17 knockout mutant as a comparison, as it does not grow at 65 °C. The average doubling time of the triplicates and their standard error can be seen in Figure 10. The standard error was calculated using Excel's T-Test function, as described in the Methodology section. Wild type HB27 had a doubling time of 47 minutes with a standard error of 5 minutes. The bS20 deletion mutant with the expression plasmid, BML117, was able to grow similar to that of wild type. Its doubling time average was 55.7 minutes and had a standard error of 7.7. Based on a T-test performed using the Excel function, there was no statistical significance between the complemented mutant and the wild-type. This means the plasmid was able to repair the growth defect seen in the bS20 deletion mutant.

The bS20 deletion mutant, BML43, had a doubling time of 281 minutes with a standard error of 65.9. This high variability in growth of the mutant may be indicative of some genetic instability, with possible secondary suppressor mutations

arising in the population at different times during growth of the culture. This means that when mutations acquire secondary suppressor mutations early on, their doubling times will be quicker, while those that acquire secondary suppressor mutations later on have longer doubling times. This has been seen in previous studies mentioned in the background paragraph and will be investigated in future studies using whole genome sequencing of multiple isolates and evolution experimentation.

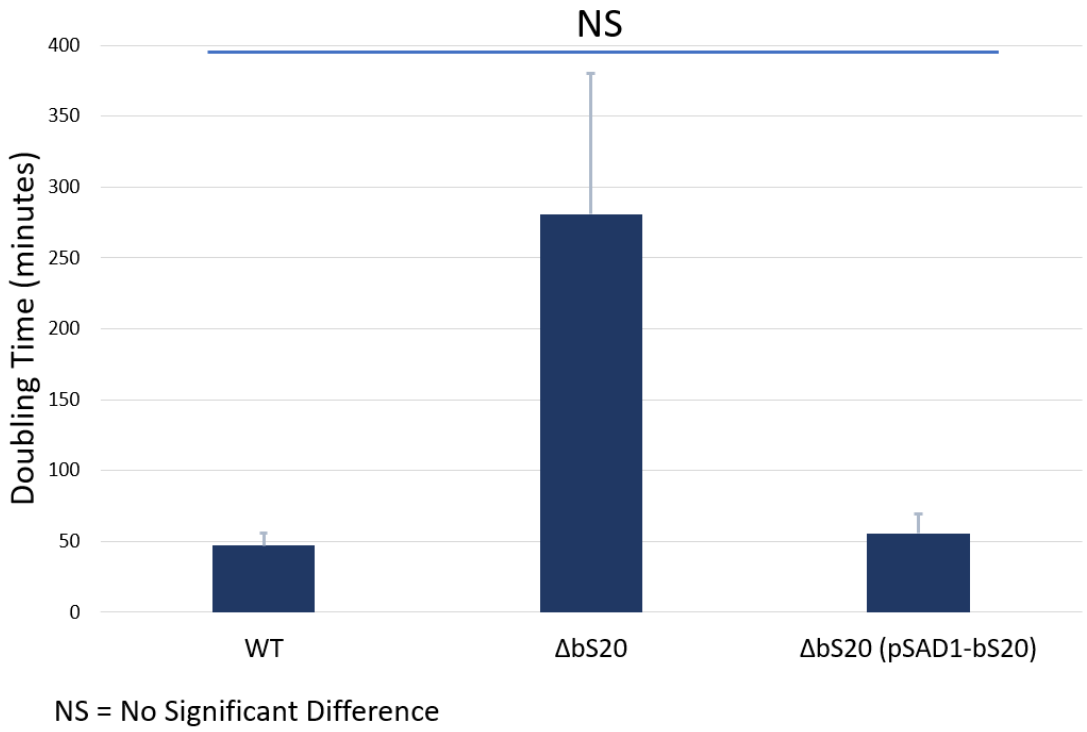

Figure 10. Growth phenotype of the Δ*rpsT::htk* deletion mutation. Bars show the average; experiments were done in triplicate. Error bars were made using the standard error custom to each mutant. The samples were each grown in TEM media at 65°C from stationary to end-stage log phase, measured by OD_{600} to 0.8. There was no statistically significant difference between the wild type and complementation mutant strain doubling times based on T-tests. There was a significant difference between the wild type and bS20 deletion mutant doubling times.

This makes additional growth rate measurements unlikely to be informative since populations would be genetically non-uniform. Prior to further growth rate analysis, whole genome sequencing should be performed to identify possible suppressor mutations. Nevertheless, I can conclude from these observations that loss of bS20 produces a severe growth defect.

Antibiotic disc diffusion assays

Previous studies have suggested that antibiotics that inhibit protein synthesis also inhibit ribosomal subunit assembly. The effect on assembly is now thought to indirectly result from protein synthesis inhibition. This led me to the hypothesis that mutants with subunit assembly defects might be hypersensitive to protein synthesis inhibitors. To test this hypothesis, I assessed the sensitivity of the *rpsT* deletion mutant to a number of antibiotics using a disc diffusion assay. The antibiotics used and their mechanisms of action can be seen in Table 4 below. Assays were performed in triplicate and wild type *T. thermophilus* HB27 was used for comparison.

Discs were made to have 100 µg of antibiotic on each, except ampicillin which was made with 10 µg of antibiotic. The plates were grown in 65 °C and checked every day, with the wild type plates growing faster than the bS20 deletion mutant plates. A variety of antibiotics were used to assess the impact of various antibiotic classes. Since bS20 was replaced with a kanamycin resistance gene, kanamycin was used as a negative control. A list of these antibiotics and their target sites can be found in Table 4 (information found via DrugBank and NIH). When the cells were grown, a ruler was used to measure the zone of inhibition in cm and

converted to mm. The averages and their standard deviation were determined and can be seen in Figure 11.

While the bS20-minus mutant was shown to be hypersensitive to some antibiotics, there were many antibiotics to which it either showed less sensitivity or had no significant difference from the wild type strain. Thus, no emerging pattern of hypersensitivity indicative of an assembly defect was evident. A larger variety of antibiotic or disc concentrations can be used for further testing if needed.

Table 4. Antibiotics: Their Drug Class, Targets, and M.O.A.

Antibiotic	Class	Target	Mechanism of Action
Kanamycin (Kan)	Aminoglycoside	30S subunit 16S rRNA & a protein 12 amino acid.	Induces mistranslation
Paromomycin (Par)	Aminoglycoside	30S subunit 16S rRNA.	Induces mistranslation
Streptomycin (Str)	Aminoglycoside	30S subunit 16S rRNA.	Induces mistranslation
Capreomycin (Cap)	tuberactinomycin	70S ribosome subunit interface	Inhibits the translocation step
Chloramphenicol (Chl)	N/A	50S subunit PTC (23S rRNA).	Inhibits peptide bond formation. May perturb nascent polypeptide exiting.
Tylosin (Tyl)	16-atom Macrolide	50S subunit peptide exit tunnel	Inhibits peptide bond formation; Blocks polypeptide exit channel
Erythromycin (Ery)	14-atom Macrolide	50S subunit 23S rRNA	Blocks polypeptide exit channel
Azithromycin (Azm)	14-atom Macrolide	50S subunit 23S rRNA	Blocks polypeptide exit channel

Lincomycin (Lnc)	Lincosamide	50S subunit PTC (23S rRNA)	Inhibits peptide bond formation
Ampicillin (Amp)	β-lactam	Cell wall	Inhibits synthesis of bacterial cell wall by inhibiting peptidoglycan synthesis at transpeptidation step.
Rifampicin (Rif)	Rifamycin	RNA polymerase β-subunit	Prevents elongation of RNA chain, prevents RNA synthesis initiation.
Thiostrepton (Thio)	Thiopeptide	GTPase-associated center of ribosome	Disrupts EF-Tu and EF-G function and ReIA binding
Levofloxacin (Levo)	Fluoroquinolones	DNA gyrase	Inhibits DNA synthesis. Promotes DNA strand breakage
Ofloxacin (Oflo)	Fluoroquinolones	DNA gyrase	Blocks growth and repair enzymes. Blocks DNA synthesis

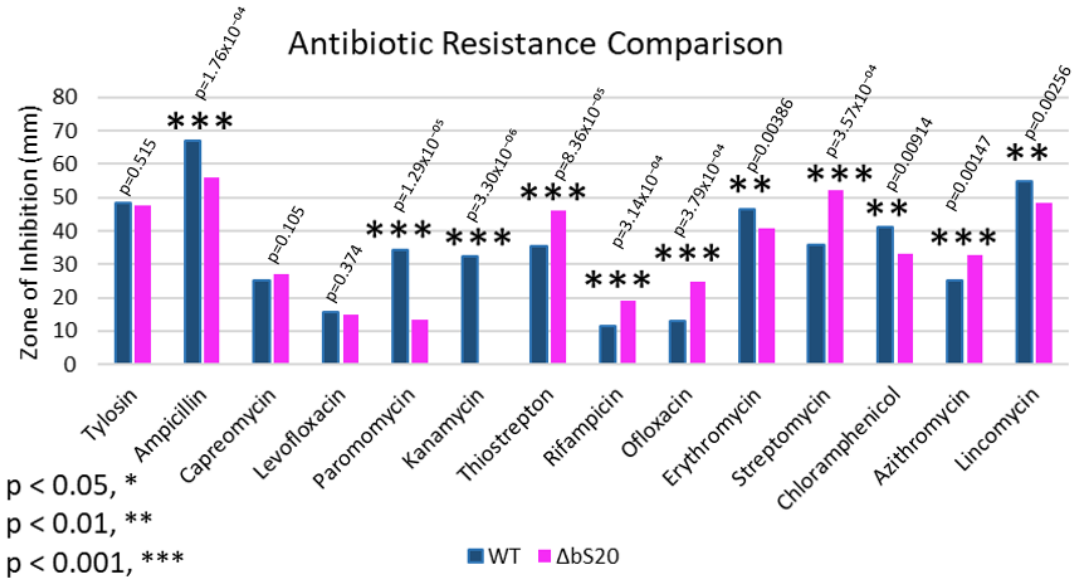

Figure 11. Bar graph showing average zones of inhibition of wild type and bS20 knockout strains in antibiotic presence. Bars show the average; experiments were done in triplicate. The samples were each grown on TEM media plates at 65°C in the presence of 5mm discs covered with antibiotic. Statistical significance between the wild type and deletion mutant strain zones of inhibition were determined using the Excel T-test function. No asterisk, no statistical significance; p<0.05 was denoted by one asterisk; p<0.01 was denoted by two asterisks, and p<0.001 three asterisks.

Statistical analysis

The antibiotic disc diffusion data was analyzed using the T-test function on Excel comparing the wild type zones of inhibition to the ΔbS20 zones of inhibition using a two-tail type 2 t-test (=T.TEST (array1, array2, 2, 2). A type 2 test (equal variance) was used instead of a type 3 test (unequal variance) because the ratio of the larger to smaller deviation was not greater than 2, so equal variance test should be used (thebmj). The growth rate data was also compared between wild

type doubling times versus the deletion mutant or complementary mutant doubling times. There was too much heteroscedasticity between the wild type and deletion mutant doubling time, so an Anova test was not used. There was not enough statistical power to perform a Kruskal Wallis or Welch's T-test. Therefore, statistical significance testing was not performed on the wild type versus deletion mutant, but based on visualization there is a large difference between the two doubling times. However, when looking at the wild type versus the complementation mutant, a Barlett test showed that there was enough equal variance between the doubling times to use a regular T test, same as used with the antibiotic disc diffusion assay. Statistical significance was denoted by the presence or absence of asterisks. No asterisks means that there is no significant difference, one asterisks means $p<0.05$, two asterisks means $p<0.01$, and three asterisks means $p<0.001$.

Complementation with pSAD1-bS20-Thx expression plasmid

To ensure that any phenotypes present in the bS20 knockout strains were in fact due to the absence of bS20, an *E. coli* expression plasmid, pSAD1 was used to try to compensate for the growth defect. Firstly, the already made BML117 used for growth rates was placed to grow at 55 °C. 65 °C, and 72 °C on plates with hygromycin B antibiotic (50 µg/uL). As a comparison, wild type HB27 and the Δ*rpsT* mutant BML43 were grown in the absence of the antibiotic at the same temperatures. HB27 and BML117 had faster growing colonies than BML43 at 65 °C and 55 °C. These plates can be seen in Figure 12. I then redid the transformation to include not just BML43 with the pSAD-bS20-Thx plasmid

(BML123) but wild type with the pSAD-bS20-Thx as well (BML127). I also transformed both BML43 with a pSAD1 empty vector (BML118) and HB27 with a pSAD1 empty vector (BML125). These were all grown in the presence of hygromycin B at 55 °C and 65 °C. All four samples were able to grow overnight at 55 °C and 65 °C. The 55 °C and 65 °C plates can be seen in Figure 13. These plates support the growth rates in their finding that the expression plasmid is able to rescue the growth phenotype.

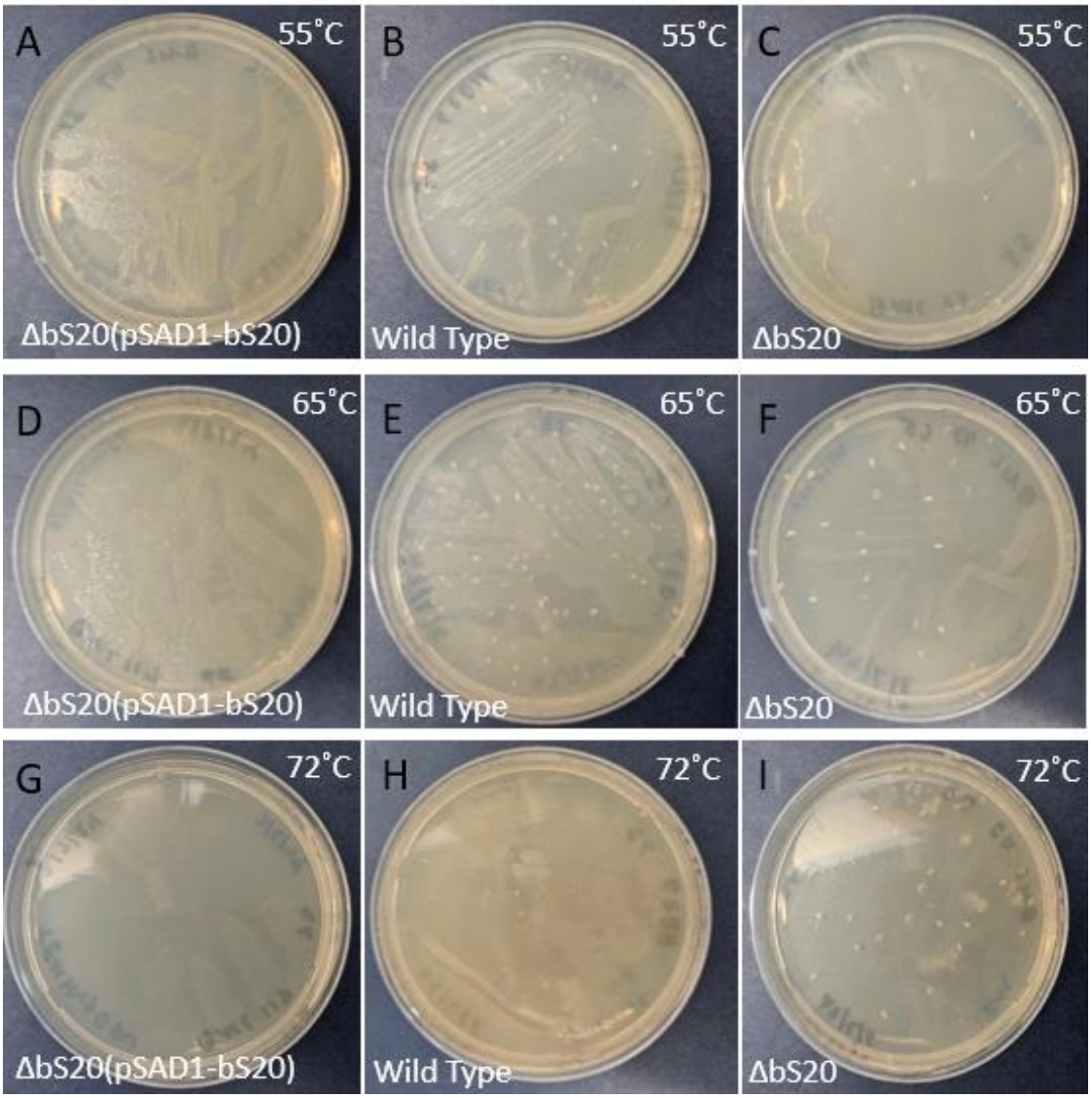

Figure 12. ΔbS20(pSAD1-bS20), wild type, and ΔbS20 growth at various temperatures. (A-C) Plate images comparing the growth of ΔbS20(pSAD1-bS20) (BML117), wild type (HB27), and ΔbS20 (BML43) at 55˚C. (D-F) Plate images comparing the growth of ΔbS20(pSAD1-bS20), wild type, and ΔbS20 at 65˚C. (G-I) Plate images comparing the growth of ΔbS20(pSAD1-bS20), wild type, and ΔbS20 at 72˚C. All strains were able to grow at 55˚C and 65˚C. ΔbS20 was not able to grow at 72˚C, but wild type and ΔbS20(pSAD1-bS20) were. This showed that the bS20 knockout mutant did not have a temperature sensitivity but did take longer than the ΔbS20 and wild type strains to grow colonies.

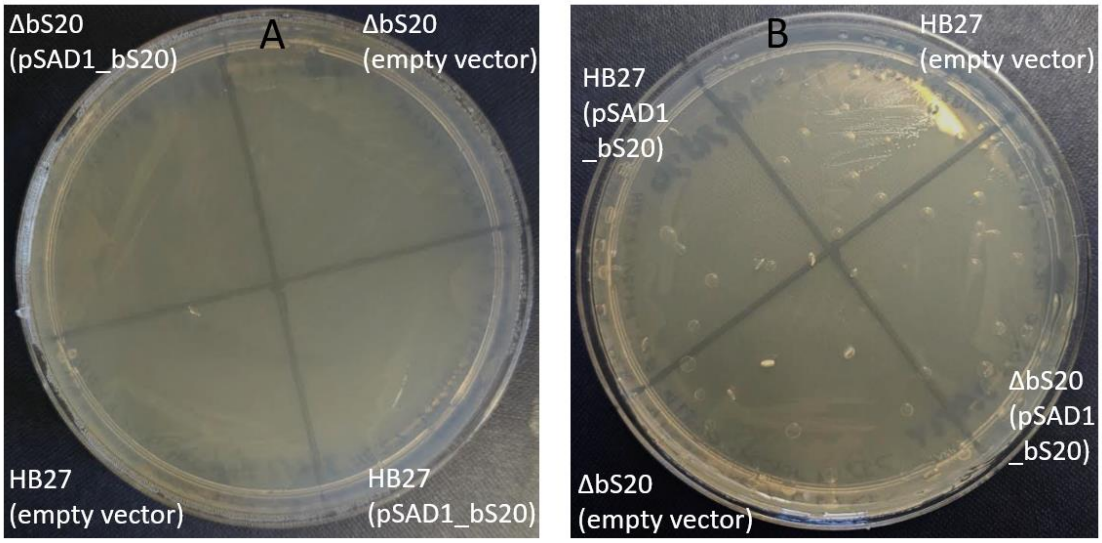

Figure 13. ΔbS20(pSAD1_bS20) and wild type complementation growth at 55 and 65˚C. (A-B) Plate image comparing the growth of wild type with the expression plasmid (pSAD-bS20-Thx), wild type with the empty vector (pSAD1), ΔbS20 with the expression plasmid (pSAD-bS20-Thx), and ΔbS20 with the empty vector (pSAD1) at 55˚C and 65˚C, respectively. All plates were able to grow at 55˚C and 65˚C. They were all able to grow quicker than the ΔbS20 mutant.

Structural analysis

To try to explain the phenotypes found both in previous studies and with my deletion mutant, I carried out an analysis of bS20 and its surrounding rRNA and r-proteins within an X-ray crystal structure of the 30S ribosomal subunit (PDB entry 6CAQ; unpublished). This allowed me to make connections between the deletion mutant phenotypes and bS20's location within the 30S subunit. I identified a number of potential sites of interactions between bS20 and 16S rRNA helices h6, h7, h8, h9, h10, h11, and h13. These helices are all part of the 16S rRNA 5' domain and these interactions can be predicted to serve to stabilize the local fold of this domain. A set of long-range interactions involving 16S rRNA helix h44 in the 3' minor domain are the only interactions that might be involved in global RNA folding. This helix is the last major secondary structure element to be formed during 16S rRNA synthesis. Formation of the bS20-h44 interaction is therefore likely a very late assembly event. This stands in contrast to the role of uS17, which we predict involves a very early binding event to the 16S rRNA 5' domain, followed by recruitment of the central domain in a major folding event. We speculate that bS20 contributes to this major folding event by stabilizing the local conformation of the 5' domain, necessary for recruitment of the central domain.

A cutoff distance of 3.0 Å was chosen, as the ideal distance for hydrogen bonds is 2.8 Å with anything above 3Å as suspect. No interactions between bS20 and other r-proteins were observed within the cutoff distance. There were, however, 21 interactions within this cutoff distance found between bS20 and the 16S rRNA. Of these interactions, only three were with bases and the other 18 were with

the RNA backbone. This indicates that global structure is recognized more efficiently than sequence specificity. bS20 needs to recognize certain features of the RNA backbone to form correct bS20-16S rRNA interactions and help the ribosome to assemble correctly. There were seven bonds found to be within 2.8 Å. All of these bonds connected a phosphate in the 16S rRNA backbone to amino acids with both charged and uncharged side chains. The 16S rRNA bound to the guanidinium of three arginine side chains, the β-hydroxybutyric acid of two serine side chains, and the ε-NH3 of a lysine side chain. All of these are highly polar, which makes sense as hydrogen bonds don't include nonpolar molecules as they don't have permanent dipoles. There were also a variety of bonds with both longer and shorter distances that the optimal 2.8 Å, which can be seen described in Table 5 below.

Table 5. Ribosomal protein bS20-16S rRNA interactions in the *T. thermophilus* 30S subunit (PDB entry 6CAQ; 3.4 Å resolution).

bS20	16S rRNA	Distance (Å)	Description
Gly`102/O	G`191/O2'	2.3	Glycine backbone carbonyl oxygen to ribose 2' OH
Arg`17/NH1	C`103/OP1	2.4	Arginine guanidinium to phosphate OP1
Lys`29/NZ	C`176/OP1	2.4	Lysine ε-NH_3 to phosphate OP1
Thr`35/OG1	G`1455/OP1	2.4	Threonine β-OH to phosphate OP1
Arg`79/NH2	U`261/OP2	2.7	Arginine guanidinium to phosphate OP2
Ser`105/OG	C`187/N3	2.7	Serine β-OH to cytosine N3
Arg`17/NH2	G`102/OP1	2.8	Arginine guanidinium to phosphate OP1
Arg`22/NH1	G`324/OP1	2.8	Arginine guanidinium to phosphate OP1
Ser`31/OG	C`1459/OP1	2.8	Serine β-OH to phosphate OP1
Lys`38/NZ	C`1439/OP1	2.8	Lysine ε-NH_3 to phosphate OP1
Ser`82/OG	C`187/OP1	2.8	Serine β-OH to phosphate OP1
Arg`83/NE	G`259/OP2	2.8	Arginine guanidinium to phosphate OP2
Lys`87/NZ	G`259/OP1	2.8	Lysine ε-NH_3 to phosphate OP1
Lys`38/NZ	C`1439/OP2	2.9	Lysine ε-NH_3 to phosphate OP2
Met`85/SD	C`186/O2'	2.9	Methionine sulfur to ribose 2' OH
Glu`60/OE1	C`193/O4'	3.0	Glutamate carboxyl oxygen to ribose 4' OH
Arg`89/NE	C`187/O2'	3.0	Arginine guanidinium to ribose 2' OH
Gly`101/O	G`191/O2'	3.0	Glycine backbone carbonyl to ribose 2'-OH
Gly`103/O	G`191/N2	3.0	Glycine backbone carbonyl to Guanine N2-amino
Leu`104/O	G`191/O2'	3.0	Leucine backbone carbonyl to ribose 2'-OH
Ser`105/N	C`187/O2	3.0	Serine α-amino to Cytosine carbonyl oxygen

CHAPTER 4

Discussion

Summary

Ribosome assembly has to be able to create tens of thousands of ribosomes as accurately and efficiently as possible. This is a large investment for the cell, and any inaccuracies can lead to defective or inhibited protein synthesis. Despite how important this is, there is still much unknown about how the ribosome is able to assembly in such a way. The overall goal of this thesis was to investigate the role of ribosomal protein bS20 in helping the formation of the 30S subunit tertiary structure. Prior to this thesis, there were no publications of this protein being removed in a thermophile like *T. thermophilus,* only in mesophiles like *E. coli* and *S. enterica.* It was shown to cause a growth defect phenotype in these mesophilic strains (Aulin *et al.,* 1993; Tobin *et al.,* 2010). I was able to use the thermophile's natural competence to successfully make a deletion of the protein bS20 as well as use the ribosome crystal structures to make predictions and interpret results.

Characterizing the Δ*rpsT* deletion strain lacking bS20

I analyzed the *rpsT* deletion mutant I made in *T. thermophilus* by performing antibiotic disc diffusion assays and growth rate comparisons. Since the uS17 deletion strain is too slow growing and temperature sensitive to perform antibiotic disc diffusion assays, this was an experiment of great interest, as the bS20 mutant was sufficiently robust for said assays. The assays were done using a various class of antibiotics, each with their own unique mechanisms of action. By using the

wild-type strain as a control, I was also able to look into the stability of the deletion mutant based on the zones of inhibition. I also used kanamycin as a negative control to show that the bS20 protein is in fact replaced by *htk* as it now has a kanamycin resistance, unlike wild type. The increase in resistance to paromomycin could possibly be attributed to the *htk* gene and the structural relatedness of paromomycin and kanamycin. Conversely, the *rpsT* deletion mutant was much more sensitive to streptomycin than the wild type; we already know that *htk* does not confer streptomycin resistance. I conclude that there is no general trend toward hypersensitivity to ribosome-specific antibiotics, inconsistent with my original hypothesis.

With the growth rates and growth comparisons, the Δ*rpsT* mutant was shown to have a growth defect, in agreement with previous research done in mesophiles. There was a large standard deviation between the three growth rates, which could be due to the bS20 knockout mutant cells readily gaining secondary suppressor mutants at various points in their growth. As seen in the plate figures above, the bS20 deletion mutant was able to grow at all three temperatures, 55, 65, and 72 °C. This is In contrast with the deletion of another primary binding protein in the 5' domain, uS17, done by my lab which cannot grow at 65 or 72 °C and takes a considerably longer time to grow at 55 °C.

While there is much to be done to characterize the bS20 mutants, this thesis helps to set the groundwork for further testing. The first step when trying to remove a protein is to make sure that the protein is non-essential. I was able to show that it is in fact not essential in our model organism *Thermus thermophilus.* These data

also show that there is no temperature-sensitive phenotype, but there is indeed a growth defect. The construction of the bS20-minus mutant and a bS20 expression plasmid lay the groundwork for further, more detailed mutational analysis of bS20 and its role in ribosome structure, function, and assembly. However, taking into account the failure of bS20 to efficiently assemble in the uS17-deficient strain, my observations are consistent with a role for both uS17 and bS20 in contributing to the folding of the 5' domain, while uS17 alone is responsible for the recruitment of the central domain. Further, as described below, bS20 may be important for stabilizing a long-range interaction with helix h44 in the 3' domain.

Streptomycin hypersensitivity

A curious outcome of antibiotic testing was hypersensitivity of the bS20 deletion mutant to streptomycin. The bS20 protein has its only interdomain interactions with the bottom of helix h44 in the 3’ domain (Aseev *et al.,* 2024). Helix h44 is the site of the decoding center, making it important for translation (Hobbie *et al.,* 2007). Streptomycin contacts helix h44 at positions C1490 and G1491 via back-bone interactions and causes increased misreading of the genetic code (Carter *et al*., 2001). This is far from the interaction of helix h44 with bS20 (Figure 14).

Using X-ray crystallography, the impact of streptomycin in the 30S ribosomal subunit of *Thermus thermophilus* has been elucidated. Streptomycin binds close to the site of codon recognition and distorts the 16S rRNA. It destabilizes the cognate anticodon stem-loop analogues but improves recognition of a near-cognate

anticodon stem-loop analogue which causes this increased misreading during translation (Demirci *et al.,* 2013).

Ribosomal protein uS12 which sits directly next to helix h44 and is contacted by streptomycin, has been implicated in a streptomycin dependence phenotype (Gregory *et al.,* 2005). The uS12 protein and the decoding site collaborate for optimized codon recognition and substrate discrimination during early tRNA selection (Demirci, *et al.,* 2013*).* The streptomycin-dependence mutations in uS12 interfere with tRNA selection by impairing GTPase activation of EF-Tu due to conformational changes to the decoding site. Mutations in this protein give abnormally low error frequency (Bohman *et al.,* 1984) and decreased miscoding (Ozaki *et al.,* 1969).

Research has found that a C to U single base substitution at position 1469 of helix h44 in *E. coli* is able to suppress streptomycin dependence mutations in uS12 and cause translational miscoding (Allen & Noller, 1991). The mutation also had a growth defect shown in the smaller colony sizes on solid media and a doubling time increase by a factor of 2. The streptomycin dependence due to uS12 mutations can also be compensated by increased miscoding conferred by mutations in proteins uS4 and uS5 (Birge & Kurland, 1970; Hasenbank *et al.*, 1973).

All this research has shown that mutations to the bottom of helix h44 can have propagating effects that induce misreading of translation in the decoding site at the top of helix h44. This has also been shown in bS20 mutations in mesophiles (Aulin *et al.,* 1993). Given this information, I hypothesize that because bS20 mutations

have been shown to induce this misreading and streptomycin also causes misreading, a bS20 deletion mutant would be hypersensitive to streptomycin.

The analysis of interactions between bS20-16S rRNA showed four interactions with the bottom of helix h44 (positions 1455, 1439, and 1459). This can cause propagating effects that would explain the defects in translation initiation, increased readthrough of stop codons, and increased efficiency of tRNA nonsense suppressors by effects on the decoding site at the top of helix h44. This already increased misreading would also explain the hypersensitivity of my deletion mutant to streptomycin. Lastly, because helix h44 is the location of multiple sites of contact between the 50S and 30S subunit (Figure 14). These propagating effects also explain the impaired 30-50S subunit association which would lead to decrease in 70S ribosomes being formed, and the growth defect. The unaffected elongation rate shows that bS20 mutants cause translation initiation defects as opposed to translation elongation defects.

16S rRNA residues A1492 and A1493 are directly involved in codon recognition. Streptomycin, paromomycin, and capreomycin all bind to the decoding site (Figure 15) and all cause misreading, but they do so by distinct mechanisms. Streptomycin stabilizes the closed conformation of the 30S subunit leading to productive binding of near-cognate aa-tRNA (Ogle et al., 2001; Demirci et al., 2013). It does so by stabilizing interactions between ribosomal protein uS12 and helix h44. In contrast, paromomycin induces a productive conformation of A1492 and A1493, driving forward near-cognate aa-tRNA binding, but without affecting domain closure (Ogle et al., 2001). Capreomycin induces misreading by an unknown

mechanism, but binds to both the 30S and 50S subunits, and does not evidently affect domain closure (Stanley et al., 2010). The specific hypersensitivity to streptomycin could therefore be an indication that the absence of bS20 perturbs decoding by affecting the dynamics of interaction between 16S helix h44 and ribosomal protein uS12.

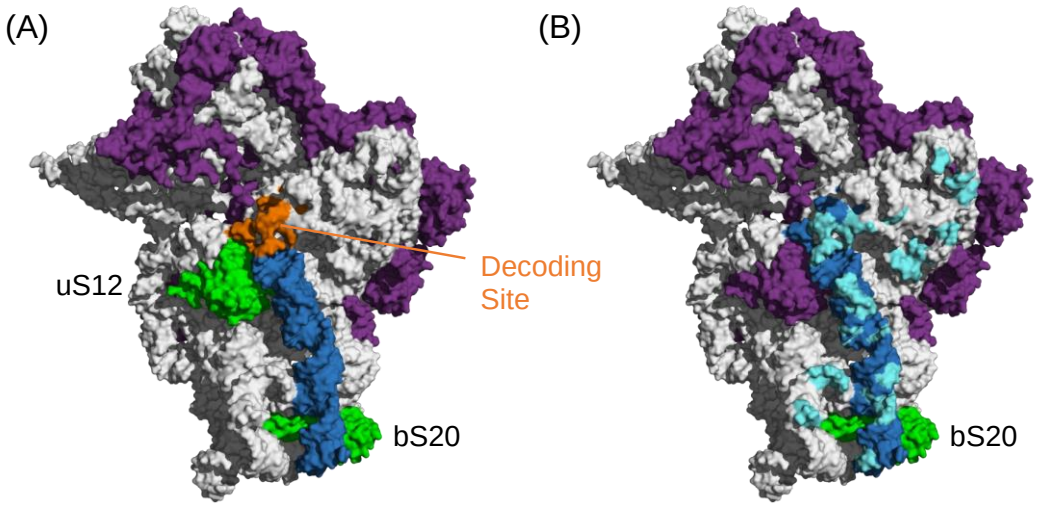

Figure 14. Potential long-range effects of bS20 deficiency. (A) The 30S subunit showing ribosomal proteins uS12 and bS20 (green), with helix h44 in skyblue and the decoding site in orange. (B) The 30S subunit showing bS20 (green) and helix h44 (skyblue). Sites of contact with the 50S subunit are shown in palecyan.

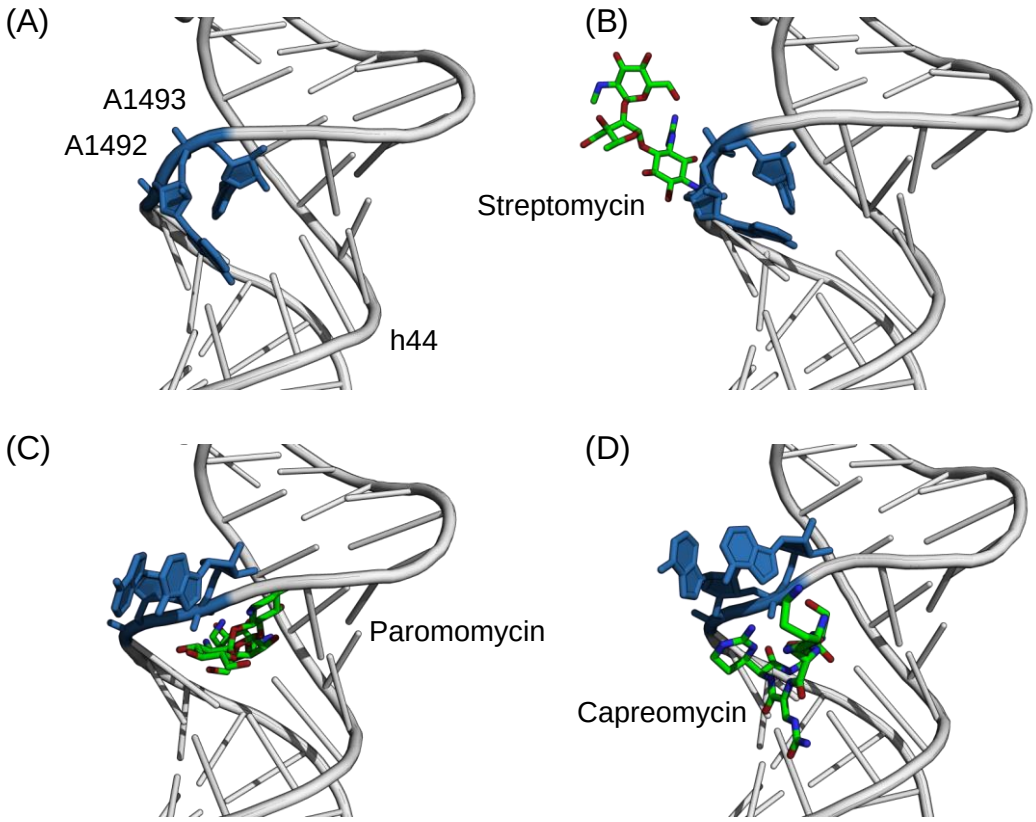

Figure 15. Antibiotics binding to 16S rRNA h44. Closeup views of the decoding site of 16S rRNA and the binding sites for aminoglycoside and tuberactinomycin antibiotics. (A) The apo 30S subunit at 3.60 Å resolution (pdb entry 4dr1; Demirci et al., 2013), (B) The 30S subunit with streptomycin bound at 3.35 Å resolution (pdb entry 4dr3; Demirci et al., 2013), (C) The 30S subunit with paromomycin bound at 3.31 Å resolution (pdb entry 1ibk; Ogle et al., 2001), and (D) The 70S ribosome with capreomycin bound at 3.45 Å resolution (pdb entry 4v7m; Stanley et al., 2010). All structures are of the *T. thermophilus* ribosome. 16S rRNA is shown as grey cartoon in ladder mode, except residues A1492 and A1493, which are shown as blue sticks/plates; antibiotics are in CPK colors except carbon atoms, which are colored green. Figure was generated using PyMOL 2.2.0.

Future directions

More in depth analyses need to be performed to look into what is happening to the ribosome structure itself before going into further experimentation. It is important to first confirm if there is both a functional and assembly defect seen in this deletion mutant. The data both in this thesis and in past studies (Dabbs, 1978; Gotz *et al.,* 1990; Aulin *et al.,* 1993) have pointed to a clear functional defect related to translation initiation defects, increased misreading of the stop codon, and impaired 30S-50S subunit association. We believe there is also an assembly defect, but that has yet to be confirmed through further testing.

To look into potential assembly defects, it is prudent to perform sucrose density gradient sedimentation. This will help to determine if the growth defect is due to an assembly problem as well as a functional defect. An analysis of the peaks at various magnesium will be done as well to determine if there is a particle similar to the 20S particle found in the uS17-minus mutant (Adilakshmi, *et al.,* 2008). If there is, 2D gel electrophoresis or mass spectrometry can be used to see if there are any other proteins missing or reduced. One protein that I predict might be affected is bS16, as it requires bS20 alongside uS4 and uS17 to bind. There has been research that point mutations with bS20 deficiency also showed deficiency in 30S proteins bS1, uS2, uS12, and bS21 in *Salmonella enterica* (Knoppel *et al.,* 2020). This study also found that mutations in the *fis* and *rpoA* genes, which encode the global regulator Fis and the C-terminal domain of the RNA polymerase α subunit were able to restore the bS20 levels. It would be interesting to see if these proteins are also deficient in a bS20 deletion mutant in a thermophile and if mutations in

the *fis* and *rpoA* genes are able to rescue any phenotypes. Once the sucrose density gradient sedimentation has been performed, this protein content can be assessed using 2D gel electrophoresis and mass spectrometry.

On the other hand, to further investigate the functional defects, the next steps would be to make and purify full ribosomes before doing *in vitro* protein synthesis. A mutant with both bS20 and uS17 could be made as well to see if it would be lethal or not.

To further look into the streptomycin effect, a killing curve can be performed. More antibiotic disc assays using a larger variety of aminoglycosides will be performed as well. More disc diffusion assays using streptomycin will be performed to have higher statistical power when comparing its effect on wild type versus the bS20 knockout. It would also be interesting to transform already characterized mutants that either cause streptomycin dependence or suppress this streptomycin dependence with gDNA from the Δ*rpsT*::*htk* mutant. These transformations can then be subjected to disc diffusion assays in the presence of various antibiotics including streptomycin.

Our current view of bS20's role in ribosome assembly, structure, and function, is to initially bind to the 16S rRNA 5' domain, where it may assist in folding of the domain. At a late stage in assembly, bS20 forms long-range interactions with the bottom of 16S rRNA helix h44, near the terminal loop. The loss of this latter set of interactions may destabilize the positioning of helix h44. Previous observations by others that mutations in bS20 affect 30S-50S association and decoding fidelity suggest that structural defects in bS20-h44 interactions are propagated up the

entire helix to the decoding site. My observation of increased sensitivity to streptomycin, which acts by causing translation misreading, is consistent with defects in the decoding site. This observation warrants further investigation. Deletions of the terminal loop of helix 44 can be made to determine if a phenotype is produced similar to that found in the bS20 mutations and deletions.

Lastly, I would want to look at secondary-site suppressor mutants. This can be done by performing experimental evolution to check for these secondary mutants at various stages of the cell's growth. Whole genome sequencing will also be performed to determine where in the genome these secondary suppressor mutants appear. To do this, a series of overnight cultures will be grown and diluted for 10-50 generations. Each culture will be streaked for single faster growing colonies. From there, whole genome sequencing will be performed to identify secondary-site suppressor mutations, potentially providing further insight into the influence of bS20 on the decoding site or on ribosome assembly.

BIBLIOGRAPHY

Abeysirigunawardena, S.C., Kim, H., Lai, J., Ragunathan, K., Rappé, M.C., Lu they-Schulten, Z., Ha, T., & Woodson, S.A.. “Evolution of protein-coupled RNA dynamics during hierarchical assembly of ribosomal complexes,” in *Na ture Communications,* 8, 492, 08 Sep. 2017.

Adilakshmi, T., Bellur, D.L., & Woodson, S.A., “Concurrent nucleation of 16S folding and induced fit in 30S ribosome assembly,” *Nature*, 455, 10 Sep. 2008, pp: 1268-1272.

Aleksandrova, E.V., Wu, K.J.Y., Tresco, B.I.B., Syroegin, E.A., Killeavy, E.E., Balasanyants, S.M., Svetlov, M.S., Gregory, S.T., Atkinson, G.C., Myers, A.G., & Polikanov, Y.S., “Structural basis of Cfr-mediated antimicrobial re-sistance and mechanisms to evade it,” in *Nature Chemical Biology,* 18 Jan. 2024

Allen, P.N., & Noller, H.F., “A single base substitution in 16S ribosomal RNA sup presses streptomycin dependence and increases the frequency of transla-tional errors,” in *Cell*, 66, 1, 12 Jul. 1991, pp: 141-148.

Aseev, L.V., Koledinskaya, L.S., & Boni, I.V., “Extraribosomal Functions of Bacte rial Ribosomal Proteins – An Update, 2023,” in *International Journal of Molec-ular Science,* 25, 5, Mar. 2024, pp: 2957.

Aulin, M., Shaoping, Z., Kylsten, P., & Isaksson, L.A., “Ribosome activity and modification of 16S RNA are influenced by deletion of ribosomal protein S20,” in *Molecular Microbiology*, 7, 6, Mar. 1993, pp: 983-992.

Baba, T., Ara, T., Hasegawa, M., Takai, Y., Okumura, Y., Baba, M., Datsenko,

K., Tomita, M., Wanner, B., & Mori, H., “Construction of *Escherichia coli* K-12 in-frame, single-gene knockout mutants: the Keio collection,” in *Molecular Systems Biology,* 21 Feb. 2006.

Birge, E.A., & Kurland, C.G., “Reversion of a streptomycin-dependent strain of *Escherichia coli*,” in *Molecular & General Genetics,* 109, 4, 1970, pp: 356-369.

Bohman, K., Ruusala, T., Jelenc, P.C., & Kurland, C.G., “Kinetic impairment of restrictive streptomycin-resistant ribosomes,” in *Molecular and General Genetics,* 198, Dec. 1984, pp: 90-99.

Brock, T.D., & Freeze, H., “*Thermus aquaticus* gen. n. and sp. n., a Nonsporulating Extreme Thermophile,” in *Journal of Bacteriology,* 98, 1, Apr. 1969, pp: 289-297.

Brodersen, D.E., Clemons Jr, W.M., Carter, A.P., Wimberly, B.T., & Ramakrishnan, V., “Crystal structure of the 30 s ribosomal subunit from *Thermus thermophilus*: structure of the proteins and their interactions with 16 s RNA,” in *Journal of Molecular Biology,* 316, 3, 22 Feb. 2002, pp: 725-768.

Brosius, J., Palmer, M.L., Kennedy, P.J., & Noller, H.F., “Complete nucleotide sequence of the 16S ribosomal RNA gene from *Escherichia coli*,” in *Proceedings of the National Academy of Sciences of the United States of America*, 75, 10, Oct. 1978, pp: 4801-4805.

Brown, E.D., & Wright, G.D., “Antibacterial drug discovery in the resistance era,” in *Nature,* 529, 20 Jan. 2016, pp: 336-343.

Bubunenko, M., Baker, T., & Court, D.L., “Essentiality of ribosomal and transcript

tion antitermination proteins analyzed by systematic gene replacement in *Escherichia coli,"* in *Journal of Bacteriology,* 189, 7, Apr. 2007, pp: 2844-2853.

Cameron, D.M., Gregory, S.T., Thompson, K., Suh, M.J., Limbach, P.A., & Dahl berg, A.E., "*Thermus thermophilus* L11 methyltransferase, PrmA, is dispensable for growth and preferentially modifies free ribosomal protein L11 prior to ribosome assembly," in *Journal of Bacteriology,* 186, Sep. 2004, pp: 5819-5825.

Cannone, J.J., Subramanian, S., Schnare, M.N., Collet, J.R., D'Souza, L.M., Du, Y., Feng, B., Lin, N., Madabusi, L.V., Muller, K.M., Pande, N., Shang, Z., Yu, N., & Gutell, R.R., "The Comparative RNA Web (CRW) Site: an online database of comparative sequence and structure information for ribosomal, intron, and other RNAs," in *BMC Bioinformatics,* 3, 2, 17 Jan. 2002.

Carr, J.F., Danziger, M.E., Huang, A.L., Dahlberg, A.E., & Gregory, S.T., "Engi neering the genome of *Thermus thermophilus* using a counterselectable marker," in *Journal of Bacteriology*, 197, 6, Mar. 2015, pp: 1135-1144.

Carter, A.P., Clemons, W.M., Brodersen, D.E., Morgan-Warren, R.J., Wimberly, B.T., Ramakrishnan, V. "Functional insights from the structure of the 30S ribosomal subunit and its interactions with antibiotics", in *Nature*, 407, Sep. 2001, pp:340-348.

Cate, J.H., Yusupov, M.M., Yusupova, G.Z., Earnest, T.N., & Noller, H.F., "X-ray crystal structure of 70S ribosome functional complexes," in *Science,* 285, 5436, Sep. 1999, pp: 2095-2104.

Cava, F., Hidalgo, A., & Berenguer, J., "*Thermus thermophilus* as biological model," in *Extremophiles,* 13, 2, Mar. 2009, pp: 213-231.

Chen, B., Kaledhonkar, S., Sun, M., Shen, B., Lu, Z., Barnard, D., Lu, T.M., Gon zalez Jr, R.L., & Frank, J., "Structural dynamics of ribosome subunit associa-tion studied by mixing-spraying time-resolved cryogenic electron microscopy," in *Structure,* 23, 6, 02 Jun. 2015, pp: 1097-1105.

Culver, G.M., "Assembly of the 30S ribosomal subunit," in *Biopolymers,* 68, 2, 02 January 2003, pp: 234-249.

Cundliffe, E., "Antibiotic inhibitors of ribosome function," in *The Molecular Basis of Antibiotic Action,* 1981, pp: 402-545.

Cundliffe, E., & Demain, A.L., "Avoidance of suicide in antibiotic-producing mi crobes," in *Journal of Industrial Microbiology and Biotechnology,* 37, 7, Jul. 2010, pp: 643-672.

Dabbs, E.R., "Kasugamycin-dependent mutants of *Escherichia coli,"* in *Journal of Bacteriology*, 136, 3, Dec. 1978, pp: 994-1001.

Dabbs, E.R., "Mutants lacking individual ribosomal proteins as a tool to investi gate ribosomal properties," in *Biochimie,* 73, 6, Jun. 1991, pp: 639-645.

Dao, E.H., Sierra, R.G., Laksmono, H., Lemke, H.T., Alonso-Mori, R., Coey, A., Larsen, K., Baxter, E.L., Cohen, A.E., Soltis, S.M., & DeMirci, H., "Goniome-ter-based femtosecond X-ray diffraction of mutant 30S ribosomal subunit crystals" in *Structural Dynamics,* 2, 4, Jul. 2015.

Davis, J., "Cryo-EM, and mass spec reveal modular ribosome assembly," in *Cell,* 27 Jun. 2017.

D'Costa, V.M., King, C.E., Kalan, L., Morar, M., Sung, W.W.L., Schwarz. C., Forese, D., Zazula, G., Calmels, F., Deburyne, R., Golding, G.B., Poinar, H.N., & Wright, G.D., "Antibiotic resistance is ancient," in *Nature,* 477, 31 Aug. 2011, pp: 457-461.

Demirci, H., Murphy 4th, F., Belardinelli, R., Kelley, A.C., Ramakrishnan, V., Gregory, S.T., Dahlbery, A.E., & Jogl, G., "Modification of 16S ribosomal RNA by the KsgA methyltransferase restructures the 30S subunit to optimize ribosome function," in *RNA,* 16, 12, Dec. 2010, pp: 2319-2324.

Demirci, H., Murphy 4th, F., Murphy, E., Gregory, S.T., Dahlberg, A.E., & Jogl, G., "A structural basis for streptomycin-induced misreading of the genetic code", in *Nature Communications*, 4, 1355, 2013.

Frank, J., "Toward an understanding of the structural basis of translation," in *Genome Biology,* 4, 237, 19 Nov. 2003.

Fromm, S.A., O'Connor, K.M., Purdy, M., Bhatt, P.R., Loughran, G., Atkins, J.F., Jomaa, A., Mattei, S., "The translating bacterial ribosome at 1.55 Å resolution generated by cryo-EM imaging services" *Nature Communications*, 14, Feb 2023, p. 1095.

Gotz, F., Dabbs, E.R., & Gualerzi, C.O., "*Escherichia coli* 30S mutants lacking protein S20 are defective in translation initiation," in *Biochimica et biophysica acta*, 1050, 1-3, 27 Aug. 1990, pp: 93-97.

Gregory, S.T., Carr, J.F., Rodriguez-Correa, D., & Dahlberg, A.E., "Mutational Analysis of 16S and 23S rRNA Genes of *Thermus thermophilus,"* in *Journal of Bacteriology,* 01 Jul. 2005.

Gregory, S.T., & Dahlberg, A.E., “Genetic and structural analysis of base substi tutions in the central pseudoknot of *Thermus thermophilus* 16S ribosomal RNA,” in *RNA,* 15, 2, Feb. 2009, pp: 215-223.

Gregory, S.T., Demirci, H., Belardinelli, R., Monshupanee, T., Gualerzi, C., Dahl berg, A.E., & Jogl, G., “Structural and functional studies of the *Thermus thermophilus* 16S rRNA methyltransferase RsmG.” in *RNA*, 15, 9, Sep. 2009, pp: 1693-1704.

Guthrie, C., Nashimoto, H., & Nomura, M., “Structure and Function of *E. coli* Ri bosomes, VIII. Cold-Sensitive Mutants Defective in Ribosome Assembly,” in *Proceedings of the National Academy of Sciences of the United States of America,* 63, 2, 15 Jun. 1969, pp: 384-391.

Hasenbank, R., Guthrie, C., Stoffler, G., Wittmann, H.G., Rosen, L., & Apirion, D.D., “Electrophoretic and immunological studies on ribosomal proteins of 100 *Escherichia coli* revertants from streptomycin dependence,” in *Molecular and General Genetics,* 127, 1973, pp: 1-18.

Held, W.A., Mizushima, S., & Nomura, M., “Reconstitution of *Escherichia coli* 30S ribosomal subunits from purified molecular components,” in *Journal of Biological Chemistry,* 248, 16, 25 Aug. 1973, pp: 5720-5730.

Held, W.A., Ballou, B., Mizushima, S., & Nomura, M., “Assembly mapping of 30S ribosomal proteins from *Escherichia coli.* Further studies,” in *Journal of Biological Chemistry,* 249, 10, 25 May. 1974, pp: 3103-3111.

Henne, A., Bruggemann, H., Raasch, C., Wiezer, A., Hartsch, T., Liesegang, H.,

Johann, A., Lienard, T., Gohl, O., Martinez-Arias, R., Jacobi, C., Starkuviene, V., Schlenczeck, S., Dencker, S., Huber, R., Klenk, H.P., Kramer, W., Merkel, R., Gottschalk, G., & Fritz, H.J., "The genome sequence of the extreme thermophile *Thermus thermophilus,"* in *Nature Biotechnology,* 22, 04 Apr. 2004, pp: 547-553.

Hobbie, S.N., Kalapala, S.K., Akshay, S., Bruell, C., Schmidt, S., Dabow, S., Vasella, A., Sander, P., & Bottger, E.C., "Engineering the rRNA decoding site of eukaryotic cytosolic ribosomes in bacteria," in *Nucleic Acids Research,* 35, 18, 2007, pp: 6086-6093.

Hulscher, R.M., Bohon, J., Rappe, M.C., Gupta, S., D'Mello, R., Sullivan, M., Ralston, C.Y., Chance, M.R., & Woodson, S.A., "Probing the structure of ribosome assembly intermediates *in vivo* using DMS and hydroxyl radical footprinting," in *Methods,* 103, 01 Jul. 2016, pp: 49-56.

Jomaa, A., Stewart, G., Martin-Benito, J., Zielke, R., Campbell, T.L., Maddock, J.R., Brown, E.D., & Ortega, J., "Understanding ribosome assembly: the structure of *in vivo* assembled immature 30S subunits revealed by cryo-electron microscopy," in *RNA,* 17, 4, Apr. 2011, pp: 697-709.

Knoppel, A., Andersson, D.I., & Nasvall, J., "Synonymous Mutations in *rpsT* Lead to Ribosomal Assembly Defects That Can Be Compensated by Mutations in *fis* and *rpoA,"* in *Frontiers in Microbiology,* 11, 06 Mar. 2020, pp: 340.

Koyama, Y., Hoshino, T., Tomizuka, N., & Furukawa, K., "Genetic transformation of the extreme thermophilus *Thermus thermophilus* and of other *Thermus* spp," in *Journal of Bacteriology,* 166, 1, Apr. 1998, pp: 338-340.

Kristjansson, J.K., & Alfredsson, G.A., “Distribution of *Thermus* spp. in Icelandic Hot Springs and a Thermal Gradient,” in *Applied and Environmental Microbiology,* 45, 6, Jun. 1983, pp: 1785-1789.

Lake, J.A., “Ribosome structure determined by electron microscopy of *Escherichia coli* small subunits, large subunits, and monomeric ribosomes,” in *Journal of Molecular Biology,* 105, 1, 25 Jul. 1976, pp: 131-139.

Leontiadou, F., Triantafillidou, D., & Choli-Papadopoulou, T., “On the characterization of the putative S20-thx operon of *Thermus thermophilus*,” in *Biological Chemistry,* 382, 7, Jul. 2001, pp: 1001-1006.

Mackie, G.A., & Parsons, G.D., “Tandem promoters in the gene for ribosomal protein S20,” in *Journal of Biological Chemistry,* 258, 12, 25 Jun. 1983, pp: 7840-7846.

Mizushima, S., & Nomura, M., “Assembly Mapping of 30S Ribosomal Proteins from *E. coli,”* in *Nature*, 226, 27 Jun. 1970, pp: 1214-1218.

Monshupanee, T., Gregory, S.T., Douthwaite, S., Chungjatupornchai, W., & Dahlberg, A.E., “Mutations in Conserved Helix 69 of 23S rRNA of *Thermus thermophilus* That Affect Capreomycin Resistance but Not Posttranscriptional Modification,” in *Journal of Bacteriology,* 190, 23, 01 Dec. 2008, pp: 7754-7761.

Murzina, N.V., Vorozheykina, D.P., & Matvienko, N.I., “Nucleotide sequence of *Thermus thermophilus* HB8 gene coding 16S rRNA,” in *Nucleic Acids Research,* 16, 16, 25. Aug 1988, pp: 8172.

Nikolay, R., Schmidt, S., Schlomer, R., Deuerling, E., & Nierhaus, K.H., “Ribo

some Assembly as Antimicrobial Target," in *Antibiotics (Basel),* 5, 2, Jun. 2016, pp: 18.

Noeske, J., & Doudna Cate, J.H., "Structural basis for protein synthesis: Snap shots of the ribosome in motion," in *Current Opinion in Structural Biology,* 22, 6, Dec. 2012, pp: 743-749.

Noller, H.F., "RNA structure: reading the ribosome," in *Science,* 309, 5740, 02 Sep. 2005, pp: 1508-1514.

Noller, H.F., & Woese, C.R., "Secondary structure of 16S ribosomal RNA," in *Sci ence,* 212, 4493, 24 Apr. 1981, pp: 403-411.

Nomura, M., "Bacterial RIbosome," in *Bacteriology Reviews,* 34, 3, Sep. 1970, pp: 228-277.

Nomura, M., & Held, W.A., "Reconstitution of Ribosomes: Studies of Ribosome Structure, Function, and Assembly," in *Cold Spring Harbor Monograph Archive,* 4, 1974.

Ogle JM, Brodersen DE, Clemons WM Jr, Tarry MJ, Carter AP, Ramakrishnan V., "Recognition of cognate transfer RNA by the 30S ribosomal subunit", In *Science*. 292, 2001, pp: 897-902.

Oshima, T., & Imahori, K., "Description of *Thermus thermophilus* (Yoshida and Oshima) comb. nov., a Nonsporulating Thermophilic Bacterium from a Japanese Thermal Spa," in *International Journal of Systematic and Evolutionary Microbiology,* 24, 1, 01 Jan. 1974.

Ozaki, M., Mizushima, S., & Nomura, M., "Identification and functional characteri

zation of the protein controlled by the streptomycin-resistance locus in *E. coli,"* in *Nature,* 222, Apr. 1969, pp: 333-339.

Parsons, G.D., Donly, B.C., & Mackie, G.A., "Mutations in the leader sequence and initiation codon of the gene for ribosomal protein S20 (*rpsT)* affect both translational efficiency and autoregulation," in *Journal of Bacteriology,* 170, 6, Jun. 1988, pp: 2485-2492.

Peechakara, B.V., Basit, H., & Gupta, M., "Ampicillin," in *StatPearls,* 28 Aug. 2023.

Polacek, N., & Mankin, A.S., "The ribosomal peptidyl transferase center: structure, function, evolution, inhibition," in *Critical Reviews in Biochemistry and Molecular Biology,* 40, 5, Sep-Oct. 2005, pp: 285-311.

Polikanov, Y.S., Melnikov, S.V., Soll, D., & Steitz, T.A., "Structural insights into the role of rRNA modifications in protein synthesis and ribosome assembly," in *Nature Structural & Molecular Biology,* 22, 4, Apr. 2015, pp: 342-344.

Qin, B., Lauer, S.M., Balke, A., Vieira-Vieira, C.H., Burger, J., Mielke, T., Selbach, M., Scheerer, P., Spahn, C.M.T., & Nikolay, R., "Cryo-EM captures early ribosome assembly in action," in *Nature Communications,* 14, 898, 17 Feb. 2023.

Ramakrishnan, V., "Ribosome structure and the mechanism of translation," in *Cell,* 108, 4, 22 Feb. 2002, pp: 557-572.

Ramakrishnan, V., "Unraveling the structure of the ribosome (Nobel Lecture)," in *Angewandte Chemie (International ed. in English),* 49, 26, 14 Jun. 2009, pp: 4355-4380.

Ramaswamy, P., & Woodson, S.A., “Global stabilization of rRNA structure by ri bosomal proteins S4, S17, and S20,” in *Journal of Molecular Biology,* 392, 3, 25 Sep. 2009, pp: 666-677.

Sashital, D.G., Greeman, C.A., Lyumkis, D., Potter, C.S., Carragher, B., & Wil liamson, J.R., “A combined quantitative mass spectrometry and electron mi- croscopy analysis of ribosomal 30S subunit assembly in *E. coli,”* in *eLife,* 14 Oct. 2014.

Schluenzen, F., Tocilj, A., Zarivach, R., Harms, J., Gluehmann, M., Janell, D., Bashan, A., Bartels, H., Agmon, I., Franceschi, F., & Yonath, A., “Structure of functionally activated small ribosomal subunit at 3.3 angstroms resolution,” in *Cell,* 102, 5, 01 Sep. 2000, pp: 615-623.

Schmeing, T.M., & Ramakrishnan, V., “What recent ribosome structures have re vealed about the mechanism of translation,” in *Nature,* 461, 7268, 29 Oct. 2009, pp: 1234-1242.

Schroedinger, L. The PyMOL Molecular Graphics System. Version 2.2.0

Shoji, S., Dambacher, C.M., Shajani, Z., Williamson, J.R., & Schultz, P.G., “Sys tematic chromosomal deletion of bacterial ribosomal protein genes,” in *Jour- nal of Molecular Biology,* 413, 4, 04 Nov. 2011, pp: 751-761.

Siidak, T., Peil, L., Xiong, L., Mankin, A., Remme, J., & Tenson, T., “Erythromy cin- and Chloramphenicol-Induced Ribosomal Assembly Defects Are Second- ary Effects of Protein Synthesis Inhibition,” in *Antimicrobial Agents and Chemothherapy,* 53, 2, Feb. 2009, pp: 563-571.

Siidak, T., Peil, L., Donhofer, A., Tats, A., Remm, M., Wilson, D.N., Tenson, T., &

Remme, J., “Antibiotic-induced ribosomal assembly defects result from changes in the synthesis of ribosomal proteins,” in *Molecular Microbiology,* 80, 1, Apr. 2011, pp: 54-67.

Simitsopoulou, M., Avila, H., & Franceschi, F., “Ribosomal gene disruption in the extreme thermophile *Thermus thermophilus* HB8. Generation of a mutant lacking ribosomal protein S17,” in *European Journal of Biochemistry,* 266, 2, Dec. 1999, pp: 524-532.

Stanley RE, Blaha G, Grodzicki RL, Strickler MD, Steitz TA, "The structures of the anti-tuberculosis antibiotics viomycin and capreomycin bound to the 70S ribosome", In *Nature Structural and Molecular Biology*, 17, Mar. 2010, pp: 289-293

Steitz, T.A., “From the structure and function of the ribosome to new antibiotics (Nobel Lecture),” in *Angewandte Chemie (International ed. in English),* 49, 26, 14 Jun. 2009, pp: 4381-4398.

Stoffler-Meilicke, M., Dabbs, E.R., Albrecht-Ehrlich, R., & Stoffler, G., “A mutant from *Escherichia coli* which lacks ribosomal proteins S17 and L29 used to localize these two proteins on the ribosomal surface,” in *European Journal of Biochemistry,* 150, 3, 01 Aug. 1985, pp: 485-490.

Takebe, Y., Miura, A., Bedwell, D.M., Tam, M., & Nomura, M., “Increased expression of ribosomal genes during inhibition of ribosome assembly,” in *Escherichia coli,”* in *Journal of Molecular Biology,* 184, 1, 05 Jul. 1985, pp: 23-30.

Tobin, C., Sekhar Mandava, C., Ehrenberg, M., Andersson, D.I., & Sanyal, S.,

"Ribosomes lacking protein S20 are defective in mRNA binding and subunit association," in *Journal of Molecular Biology,* 397, 3, 02 Apr. 2010, pp: 767-776.

Trakhanov, S.D., Yusupov, M.M., Agalarov, S.C., Garber, M.B., Ryazantsev, S.N., Tischenko, S.V., & Shirokov, V.A., "Crystallization of 70S ribosomes and 30S ribosomal subunits from *Thermus thermophilus,"* in *FEBS Letters,* 220, 2, 17 Aug. 1987, pp: 319-322.

Trakhanov, S., Yusupov, M., Shirokov, V., Garber M., Mitschler, A., Ruff, M., Thierry, J.C., & Moras, D., "Preliminary X-ray investigation of 70S ribosome crystals from *Thermus thermophilus,"* in *Journal of Molecular Biology,* 209, 2, 20 Sep. 1989, pp: 327-328.

Vazquez, D., "Inhibitors of Protein Biosynthesis," in *Molecular Biology Biochemis try and Biophysics,* 30, 1979.

Waller, J.P., "Fractionation of the ribosomal protein from *Escherichia coli,"* in *Journal of Molecular Biology,* 10, 2, Nov. 1964, pp: 319-336.

Warner, J.R., & Gorenstein, C., "Chapter 4: The Ribosomal Proteins of *Saccha romyces cerevisiae,"* in *Methods in Cell Biology,* 20, 1978, pp: 45-60.

Watson, J.D., "The synthesis of proteins upon ribosomes," in *Bulletin de la So ciete de chimie biologique,* 46, 1964, pp: 1399-1425.

Watson, Z.L., Ward, F.R., Meheust, R., Ad, O., Schepartz, A., Banfield, J.F., and Cate, J.H., "Structure of the bacterial ribosome at 2 Å resolution," in *eLife,* 14 Sep. 2020.

Webster, S.M., May, M.B., Powell, B.M., & Davis, J.H., "Imaging structurally dy

namic ribosomes with cryogenic electron microscopy," in *ArXiv,* 30 Aug. 2023.

Williamson, J.R., "After the ribosome structures: How are the subunits assem bled?" in *RNA Society,* 9, 2003, pp: 165-167.

Wimberly, B.T., Brodersen, D.E., Clemons Jr, W.M., Morgan-Warren, R.J., Carter, A.P., Vonrhein, C., Hartsch, T., & Ramakrishnan, V., "Structure of the 30S ribosomal subunit," in *Nature*, 407, 21 Sep. 2000, pp: 327-338.

Wittmann, H.G., "Structure, Function, and Evolution of Ribosomes," in *European Journal of Biochemistry,* 61, 1975, pp: 1-13.

Woodson, S.A., "RNA folding and ribosome assembly," in *Current Opinion in Chemical Biology,* 12, 6, Dec. 2008, pp: 667-673.

Woodson, S.A., "RNA folding pathways and the self-assembly of ribosomes," in *Accounts of Chemical Research,* 44, 12, 20 Dec. 2011, pp: 1312-1319.

Yamaguchi, K., & Subramanian, A.R., "Proteomic identification of all plastid-spe cific ribosomal proteins in higher plant chloroplast 30S ribosomal subunit," in *European Journal of Biochemistry,* 270, 2, Jan. 2004, pp: 190-205.

Yonath, A., "Hibernating Bears, Antibiotics, and the Evolving Ribosome (Nobel Lecture)," in *Angewandte Chemie International Edition,* 49, 26, 09 Jun. 2009, pp: 4340-4354.

Yusupov, M.M., Yusupova, G.Z., Baucom, A., Liberman, K., Earnest, T.N., Cate, J.H., & Holler, H.F., "Crystal structure of the ribosome at 5.5 A resolution," in *Science,* 292, 5518, 04 May. 2001, pp: 883-896.